Ultrasonic Sensor-Based Mapping for an Autonomous Vehicle

Madhavan, Vinodh Raam

Award date:
2021

EINDHOVEN UNIVERSITY OF TECHNOLOGY

Department of Mechanical Engineering
Automotive Technology
Dynamics and Control Group

Ultrasonic Sensor-Based Mapping for an Autonomous Vehicle

Master Thesis

Vinodh Raam Madhavan
1362518
DC2021.007

Primary supervisor :	dr. ir. Tom. P. J. van der Sande
Supervisor and committee chair :	prof. dr. Henk Nijmeijer
Other committee member :	dr. Gijs Dubbelman

Eindhoven, January, 2021

Declaration concerning the TU/e Code of Scientific Conduct for the Master's thesis

I have read the TU/e Code of Scientific Conduct[i].

I hereby declare that my Master's thesis has been carried out in accordance with the rules of the TU/e Code of Scientific Conduct

Date 11-Jan-2021

Name Vinodh Raam Madhavan

ID-number 1362518

Signature 

Insert this document in your Master Thesis report (2nd page) and submit it on Sharepoint

[i] See: http://www.tue.nl/en/university/about-the-university/integrity/scientific-integrity/
The Netherlands Code of Conduct for Academic Practice of the VSNU can be found here also.
More information about scientific integrity is published on the websites of TU/e and VSNU

Abstract

Recent technological advancements in automotive industry have led to the development of autonomous vehicles. Autonomous vehicles are expected to drive efficiently without a driver and avoid collisions to ensure safety. To reach this goal, significant efforts are taken to solve the challenges in autonomous driving. In this regard, the first challenge for a self-driving vehicle is to perceive its surrounding environment. To perceive the surrounding environment, ultrasonic sensors play an important role of detecting obstacles in the close vicinity of the vehicle. The goal of this graduation project is to obtain an accurate map of the surrounding environment using the ultrasonic sensors.

To achieve an accurate map representation of the surrounding environment using the ultrasonic sensors, two predominantly used occupancy grid (OG) techniques are implemented. These are inverse sensor model (ISM) based OG mapping and forward sensor model (FSM) based OG mapping. The ISM-based mapping algorithm is developed using a sensor model and a recursive update equation is derived using the Bayesian method. Firstly, the ISM is constructed to interpret the occupancy information of the grid cells in terms of probability values for an obtained sensor measurement. This sensor model is constructed as a function of the cell parameters without considering the measurement aberrations. The occupancy information from multiple sensor measurements is combined by applying the Bayesian update method. One of the important assumptions made in this mapping algorithm is the independence of the occupancy states of the cells. In the FSM based approach, all characteristics of the sensor are considered and the occupancy of the map cells is considered dependent. An ultrasonic sensor measurement can be caused by three distinct events, namely random phenomenon, max-range measurement, measurement due to an obstacle. All these events are given priority for the OG mapping. In this approach, the problem of mapping is considered as a likelihood maximization of the obtained sensor measurements for various possible maps. The expectation-maximization (EM) algorithm is employed to solve this likelihood maximization problem.

In addition to the developed algorithms, a bench-marking suite with a set of metrics is developed for quantitative analysis of the mapping algorithms. To investigate the influence of the algorithm parameters on the performance of the algorithms, the metric values are analyzed. Finally, the comparison of the mapping algorithms using the metric values show that the FSM based method has a slightly better overall performance compared to the ISM based method under ideal circumstances.

Acknowledgment

Completing this thesis during the unprecedented times of Covid-19 is impossible without many people who have greatly inspired and supported me. In particular, I would like to thank my supervisor dr. ir. Tom. P. J. van der Sande for providing continuous guidance and encouragement. Your insightful comments during our discussions provided a different perspective of an approach.

I take this opportunity to express my deepest gratitude to my supervisor/mentor prof. dr. H. Nijmeijer for continuous support and timely feedback. I am grateful for your critical assessment of my work. Your thought process greatly inspires me to sharpen my thinking.

I would like to thank both my supervisors again for providing the wonderful opportunity to work on such an interesting and challenging project.

Any attempt at any level cannot be satisfactorily completed without the support of my parents and friends. I take this opportunity to thank my parents for where I am now. I would also like to thank my friends, who provided stimulating discussions as well as happy distractions to rest my mind outside of my research.

Contents

Nomenclature

List of Symbols

$\bar{H}$	Event of not reflecting the sonar beam by an obstacle
$\bar{m}$	Freeness grid map cell
Δ	Error
δ	Sensor noise
κ	Metric
μ	Mean of a normal distribution
σ^2	Variance of a normal distribution
θ	The angle made by the ray joining a cell and the sensor position with respect to the main vertical axis of the sensor cone
A	Occupancy map; area
B	Occupancy map
C	Cells in a class belonging to confusion matrix
c	Correspondence variable
D	Set of all radial distances; divergence
d	Radial distance (perpendicular) from the sensor position; exploration distance
E	Exploration points
e	Expectation variable
$E[X]$	Expectation of a random variable
$g(x)$	A function g of the variable x
H	Event of reflecting the sonar beam by an obstacle
J	Maximization function value
l	Log-odd ratio of a state; cell size

M	Occupancy grid map
m	Occupancy grid map cell
N	Number of cells
O	Occupancy state
P	Total occupied cells in the ground truth map
p	Probability parameter
$p(x)$	Probability of an event x
$p(x\|y)$	Probability of an event x conditioned that the event y already occurred
$p(x\|y,z)$	Probability of an event x conditioned that the event y and z already occurred
S	Number of sensors
s	Stance number of an occupied cell
Z	Set of all sensor measurements
z	Sensor measurement

Subscripts

emp	Empty
exp	Explorable
hit	Event of reflecting from an obstacle
i	Cell index
K	Total number of occupied cells
max	Maximum range
occ	Occupied
$rand$	Random
t	Time instance
tot	Total
v	Vehicle
x, y	Indices

Superscripts

$*$	True value
0	Initial value
n	Number of sensors
T	Final time instance

List of Abbreviations

EM Expectation Maximization.

FN False Negative.

FNR False Negative Rate.

FoV Field of View.

FP False Positive.

FPR False Positive Rate.

FSM Forward Sensor Model.

GT Ground Truth.

HMM Hidden Markov Model.

ISM Inverse Sensor Model.

MAP Maximum A Posterori.

ME Map Error.

MS Map Score.

OE Overall Error.

OG Occupancy Grid.

PAS Parking Assist System.

SLAM Simultaneous Localization and Mapping.

TN True Negative.

TNR True Negative Rate.

TP True Positive.

TPR True Positive Rate.

UR Uncertainty Rate.

Chapter 1

Introduction

Recent advancements in technology have reduced human effort on driving to a large extent [1, 2]. Over the years, passenger cars have evolved rapidly with increased comfort and reduced driving efforts [3]. This evolution has come along with the advent of sensors used for numerous applications. One of the applications of sensors is to perceive the surrounding environment to aid driving. In this research, contributions are made toward perception of the environment using sensors for autonomous driving application. To understand the problem addressed in this graduation project, Section 1.1 provides the necessary background information and the importance of environment perception for autonomous driving. Section 1.2 provides the problem description for this project and the important steps to be followed to accomplish the task of environment perception for a self-driving car. Finally, in Section 1.3, the outline of this thesis is presented.

1.1 Background

The prospect of cars driving autonomously on public roads is imminent owing to advances in robotics, computational power, communications and sensor technologies [4, 3]. The functionality of a self-driving car is categorized in a five level hierarchy for autonomous driving framed by the Society of Automotive Engineering (SAE)[5]. According to the SAE, at level 0, the driver performs all aspects of dynamic driving, i.e., zero autonomy. At level 1, the driver assist systems help in specific driving mode; however, the driver is expected to perform all the remaining aspects of the dynamic driving task. In level 2 of automation, the vehicle will be able to drive itself using the driver assistance systems, but the driver is required to remain aware of the driving conditions and be prepared to take over at any instance. At level 3, the autonomous vehicle will be able to drive for extended periods of time, however, the driver is required to take over whenever prompted by the system. Beyond level 3, the driver intervention is not required, and the system will be able to execute the fallback functionality. In level 4, the vehicle is restricted to certain conditions, whereas in the highest level, i.e., at level 5, the vehicle is capable of driving in all situations.

As a contribution to the development of autonomous driving technology, the TU/e is leading the I-Cave research program [6]. The I-Cave research program addresses the current transportation challenges on throughput and safety with an integrated approach to automated and cooperative driving [6]. Through this research program, the TU/e aims to operate a string of Renault Twizys as cooperative

and autonomous vehicles [5]. These Renault Twizys are currently equipped with radar and camera sensors for observing the surrounding environment. In addition to these sensors, ultrasonic sensors are equipped during an internship work [7] for object detection. The ultrasonic sensors, one of the main sensors in the category of time of flight [8], are equipped primarily to detect the presence of obstacles in the close vicinity of the ego vehicle. All the sensors used for perception have its own strengths and weaknesses, and each sensor cannot handle all given situations [9, 10]. For example, a radar is effective for object tracking and a camera can provide various features of an obstacle. Therefore, for a robust obstacle detection system, all the sensors can be combined.

One of the important challenges in autonomous driving is the parking maneuver as it requires driving in a cramped environment. Hence, a parking maneuver requires knowledge of the surrounding environment. Therefore, in highly cluttered environments, obstacle positions should be known precisely for collision-free execution of the parking task. In addition to the map requirement, the parking maneuver also requires accurate path planning for navigation and tracking techniques for appropriate control of the ego vehicle. Therefore, the key factors related to the aspects of an autonomous parking system are

- Building a precise map of the surrounding environment around ego car in a parking lot (cluttered environment). This is also called as the mapping problem.
- Localizing the ego car in the environment.
- Generating a collision-free path and tracking it with minimum error.

Considering the above factors to build a complete autonomous system, the first priority is to address the problem of mapping. In the absence of a precise map, there is a high chance that the other dependent tasks (path planning and tracking) could fail and lead to collision of the vehicle. In this project, the focus is on obtaining a precise map using the ultrasonic sensors. The main advantage of these ultrasonic sensors is that they provide distance information at a low cost. Moreover, fusion of information from multiple ultrasonic sensors helps to build an obstacle map [11]. Therefore, the main objective is determining a map of the environment taking into account the ultrasonic sensor characteristics. To this end, a mapping algorithm has to be developed, which will be the main topic of this thesis.

1.2 Problem Description

This research focuses on the problem of building consistent maps using the ultrasonic sensors. Therefore, the information from the other perception sensors are not considered for obstacle detection. One of the main applications of autonomous driving using ultrasonic sensors is in a parking lot, where the environment is assumed to consists of static obstacles. Hence, the problem of mapping for autonomous driving is narrowed to static environments using ultrasonic sensors. Furthermore, the problem of simultaneous localization and mapping (SLAM) is bypassed by assuming that the vehicle poses are available as an input to the mapping algorithm. Moreover, the vehicle is assumed to be controlled manually to move through the environment to be mapped.

In addition to the vehicle poses, the measurements from the ultrasonic sensor are used as an input to the mapping algorithm. These measurements indicate only the distance of the closest obstacle in

the sensor field of view (FoV); therefore, the exact position of the obstacle is not available explicitly. Another challenge with the ultrasonic sensors is to account for inconsistent measurements caused by random phenomena and measurement noise. In addition to the challenges with the inputs, the map generated as the output must meet certain requirements. The representation of the surrounding environment should provide a distinction between the occupied and the free space. Furthermore, the map representation in terms of probability is highly valuable for path planning, navigation and obstacle avoidance [12]. Finally, the mapping algorithm should be computationally efficient as a generated map is required at each step of vehicle exploration.

Based on the above described problem, the main research question of this project is formulated as:

"Which mapping algorithm provides an effective map representation of the static environment using multiple ultrasonic sensors ?"

In order to address this research question and to achieve the goal of this project, the following steps need to be accomplished.

- Identify the potential mapping algorithms and modify them for effective perception of the environment.
- Define a set of metrics to evaluate the generated maps and analyze the performance of a mapping algorithm.
- Analyze the performance of the algorithm using the metrics for various values of the parameters in the algorithm.
- Compare the algorithms for the best representation of the environment.

1.3 Outline

The approach to this project begins with the study of the state of art mapping algorithms in Chapter 2. This chapter also reviews the metrics from literature for comparing mapping algorithms. Furthermore, in Chapter 3, the characteristics of the ultrasonic sensors are studied for in-depth analysis of the input to the mapping algorithm. In Chapter 4, the methodologies chosen are modified and the mapping algorithms are framed. To evaluate the maps generated from the mapping algorithms a bench-marking suite is formulated in Chapter 5. In Chapter 6, the generated maps are analyzed and compared using the metrics defined to evaluate the performance of the mapping algorithms. Finally, conclusions and recommendations are given in Chapter 7.

Chapter 2

Literature Review

For a vehicle to park autonomously, it should be able to navigate safely through a possible complex environment. Parking assist systems (PASs) help the vehicle to achieve the goal of autonomous parking [13]. The PAS consists of four main subsystems: the state estimation, the map construction, the path planning and the tracking controller subsystem. The task of the state estimator is to determine the states of the vehicle, such as position, orientation, using sensor information. In addition to this, velocity of the vehicle and time derivatives of the velocity can also be calculated, which serve as inputs to the tracking controller subsystem. The task of the map construction subsystem is to obtain information from the sensors and identify the free parking space after drawing the map of the environment. The information of the environment map and the free parking space is sent to the path planning subsystem in order to determine the geometry of the reference path. Each of the components are dependent on each other to cooperatively achieve the goal of autonomous parking. The interaction between the components of the PAS and with the vehicle is shown in Figure 2.1

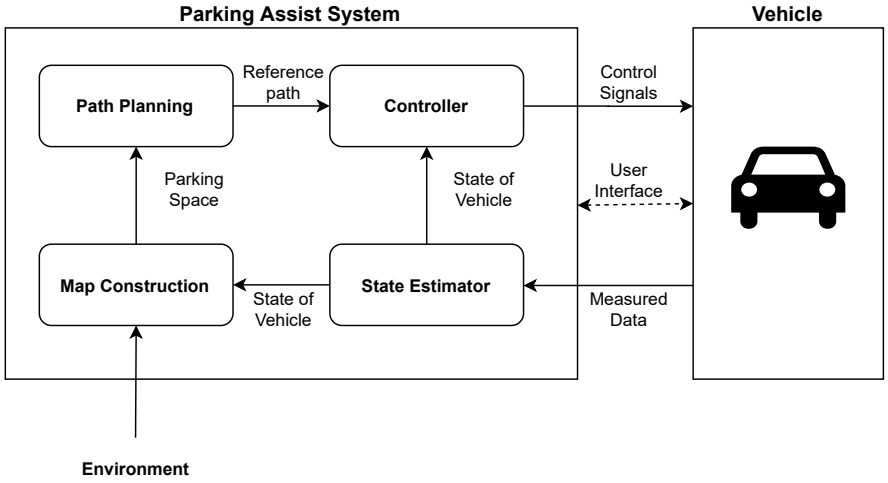

Figure 2.1: Autonomous parking system [13].

For an autonomous vehicle to move confidently in an environment, the vehicle should have a map of the environment. A map can be constructed by having the necessary information of the environment obtained through the vehicle's sensory data. This construction of a map useful for the vehicle's navig-

ation is performed by a mapping algorithm. In general, the map constructed by a mapping algorithm can be classified roughly in two categories, i.e., metric and topological maps [14]. The metric maps are detailed geometric representations of the environment. These maps provide exact co-ordinates of a point in the environment along with its features. On the other hand, the topological maps are graph-like representations of the environment considering only the places and relations between them, as shown in Figure 2.2a. In these maps, the places or landmarks are the vertices and the edges connecting them denote the relations between them. Usually the relation between two landmarks is an obstacle-free pathway. The metric maps are more finely grained in practice than the topological ones. Therefore, constructing a metric map could involve higher computation than constructing a topological map. Despite the high computation, the metric maps are highly convenient for an autonomous vehicle as they provide accurate knowledge on the occupied and free space in the environment. An example of a metric map differentiating the occupied space and free space is shown in Figure 2.2b. Furthermore, the metric maps are able to differentiate between distinct places better than the topological maps. Therefore, a metric map is the convenient way of representing an environment, which helps an autonomous vehicle to navigate.

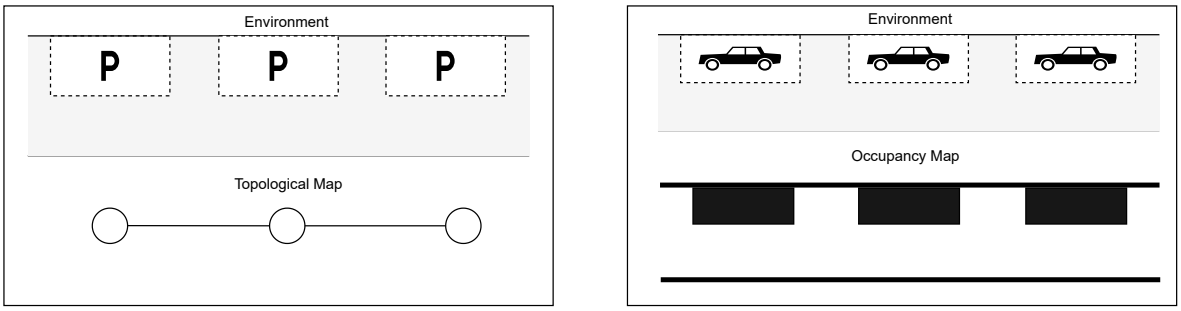

(a) (b)

Figure 2.2: Map classification [14]: (a) a topological map representing the three important places in a graph like representation, (b) an occupancy map as an example of a metric map.

In [15], several mapping algorithms for static environments are discussed and compared. Most of the algorithms discussed in [15] address the mapping problem with unknown vehicle poses. The mapping problem with the unknown poses is also called the simultaneous localization and mapping (SLAM). For the simpler case of mapping with known poses of the vehicle, the grid-based mapping algorithms have shown to generate consistent maps from noisy and incomplete sensor data. According to the problem description, the objective of this thesis is to create a map with known vehicle poses. Therefore, the grid-based mapping is a good framework for this. To this end, the forthcoming sections review the literature on the grid-based mapping algorithms.

2.1 Grid-based Mapping

The grid based approach for mapping is commonly used for obstacle detection as it is easy to translate any sensor measurement into probability distribution over the grid [10]. For multiple different sensors, occupancy grid mapping is a versatile framework to perform a low level sensor fusion methods. A low level sensor fusion processes the raw sensor data to obtain the occupancy information. By using

the raw sensor data, the information loss is prevented. These fusion methods depend on the sensor characteristics and the type of information obtained from the sensor.

A grid-based approach for mapping is a popular topic for research [16]. Among the grid-based methods of mapping, the main difference is the method of data integration for an accurate and coherent knowledge of the environment. In [16], the Bayesian, Fuzzy and Dempster-Shafer methods of data integration are investigated for a comparative study. All three methods are considered for the problem of map building for the same mobile robot with 8 ultrasonic sensors operating in the same environment. Maps constructed based on various approaches are provided in the simulation results. Based on the simulation results, it was concluded that the map constructed using the Bayesian method is more appropriate for navigation and path planning as it has more fitness to the ideal map and generated a shorter planned path. In addition to this, the other two methods led to more lengthy and dangerous routes as compared to the Bayesian generated map.

A sonar-based mapping and navigation system is developed for an autonomous mobile robot in [17]. The data collected from the sonar are interpreted as probability profiles to determine the occupancy of an area. Data from multiple measurements are used to build the occupancy map for the autonomous robot operating in an unknown and unstructured environment. The conceptual structure of an autonomous mobile robot is represented in Figure 2.3. The approach of [17] for mapping starts with obtaining the range measurements from the sonar units whose position with respect to the robot is known. These range measurements are interpreted as providing information of probably empty and somewhere occupied areas in the space subtended by the sonar beam. This occupancy information is modeled as probability profiles and as the robot moves, more data from the sonar units are integrated systematically to build the occupancy map. Overlapping the empty or occupied areas improves the map definition by sharpening the boundaries of the occupied regions. Each sonar reading provides partial evidence about a map cell being empty or occupied. Different reading asserting that a cell is empty will confirm each other, as is the case of occupied cells. On the other hand, if the readings contradict, then it weakens the certainty of the cell being occupied or empty. The final constructed map indicates the probably occupied, probably empty, and the unknown regions.

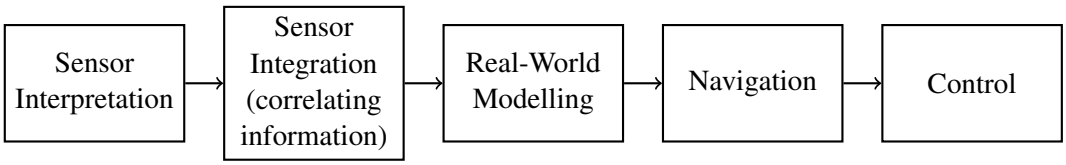

Figure 2.3: Conceptual structure of an autonomous robot [17].

The underlying formulation of the occupancy grid framework is presented in [18]. The occupancy grid (OG) is a multi-dimensional random field that maintains stochastic estimates of the occupancy state of each cell in a spatial lattice. Bayesian estimation procedures allow the incremental updating of the OG cells using the reading taken from several sensors and from multiple points of view. The OG map is a multi-dimensional tessellation of space into cells, where each cell stores a probabilistic estimate of its state. For decision making of the states, the optimal estimate is given by Maximum A Posteriori (MAP) decision rule, i.e.,

$$\begin{cases} C \text{ is OCCUPIED, if } P(s(C) = \text{ OCC }) > P(s(C) = \text{ EMP }), \\ C \text{ is EMPTY, if } P(s(C) = \text{ OCC}) < P(s(C) = \text{ EMP }), \\ C \text{ is UNKNOWN, if } P(s(C) = \text{ OCC }) = P(s(C) = \text{EMP }). \end{cases} \tag{2.1}$$

Here, the cell considered is denoted as C and its occupancy state is represented as $s(C)$. The probability that a cell's state is occupied/empty is given by $P(s(C) = OCC/EMP)$. The generated OG map using the decision rule is further used for robotic path planning avoiding all the obstacles to reach a desired position. Therefore, this method of OG based mapping presents a nice way to interpret the information from multiple sensors over multiple positions of the robot.

Further improvement on OG research came through [19] authored by Sebastian Thrun. In [19], a new algorithm is described to overcome the problem of inconsistent maps in a cluttered environment, even for noisy sensors. The paper claims that the maps generated by the new approach are more accurate than those generated using the traditional technique [18]. The paper defines inverse and forward models for generating an OG map using sonar sensors. The previous literature [17] also uses an inverse model where the OG maps are estimated from the sensor measurements. Rework of the traditional inverse model was also carried out to represent the posterior of the grid map in a log-odds form. The log-odds can be calculated recursively by estimating the posterior through the Bayes rule. The common assumption of the static world mapping is also used here to keep the mathematics simple. Hence, the past measurements are conditionally independent given the knowledge of the map. In the forward model, the likelihood of the sensor measurements of each map is calculated. Hence, the mapping becomes an optimization problem, which is the problem of finding the map that maximizes the data likelihood.

A qualitative comparison between the inverse and the forward sensor models is presented in [20]. The static assumption in the inverse model has adverse effect on the map, as the sensor readings are conditionally independent given the knowledge of only a map cell and not the complete map. In the inverse model, the large range measurements are given less weight in order to stay robust even for specular reflections. The results of experiment comparing the forward and the inverse model show that the forward model overcomes the problems in inverse model, but the computational effort is high. Therefore, both the approaches present an overall good representation of the environment with each having disadvantages of its own.

For occupancy mapping using multiple sensor of same type, a raw data fusion is applied in [21]. The advantage of using same type of sensors is that the sensor model and the frequency of the sensors remain almost same. The other method proposed is the grid-fusion, where separate grids are generated for each sensor and then fused into one single grid. If the contribution of the individual sensors are distinct, the probability from each sensor is provided a positive weight to indicate the contribution of each sensor.

The paper [22] presents a quantitative study of various approaches [23], [11], [24], [25], [19] and finally determining the best approach which is capable of creating an accurate representation of the operating environment. The five methods considered for the quantitative study are briefly explained in the following paragraphs. Finally, the results of [22] are discussed.

In the first method, Moravec and Elfes [23], the first research made on the OG maps for a mobile robot considers sonar range reading to obtain information concerning empty and occupied areas in the sensor cone. The reading obtained is modelled as probability profiles projected on to a rasterized map. However, the method fails to consider the speculation phenomenon in the sonar readings. Specular reflections lead to erroneous readings, hence labelling the cells as unoccupied incorrectly, or an unoccupied cell to be labelled as occupied. The other issue with this method is that once the probability value associated with a cell converges to a certainty of 1, the probability value associated with that cell cannot be altered by any future evidence. Despite these issues, this method successfully obtained

moderately high-resolution spatial maps of the robot's surrounding using sonar-range readings, which is further used for the robot's navigation.

The second method is from Matthies and Elfes [11]. It explains the framework of an OG map. This framework consists of developing a probabilistic sensor model, map updating model and a sensor integration model. The comparison of stereo and sonar sensor maps shows that the sonar sensors are weak in recovering the object shapes. But, with several sets of readings, the sonar is able to recover a good description of the surfaces. This method uses a single map during operation rather than an empty, occupied and integrated maps utilized in the previous method. The main disadvantage of this method is that a single update can change the occupancy value of a cell drastically which means that cell values can fluctuate. The other disadvantage is that once the cell has converged to either 0 or 1, the occupancy values cannot be changed.

The third method corresponds to Thrun proposed in the year 1993 [24]. This method uses neural networks to create an OG map. But, the limitation of this method arises from the nature of neural networks itself, i.e., it is not practically possible to train the neural network until convergence. If the training is to be done until convergence, then not just the sensor characteristics are required, but also the environmental characteristics are required to be trained. This training requires frequent update data, which also degrades generalization.

The fourth method was proposed by Konolige in 1997 [25]. This method addressed the problem of specular and redundant readings through probabilistic inference. For purposes of updating the map, the method combines the probability of the cell being occupied and empty using logarithms and additions. Experiments were carried out to test the OG update method and showed that the accuracy improved drastically as compared to [23] and [11]. Therefore, the highlight of this method is the sensor model which considers the practicality aspects of the sensor.

The fifth method [19] is quite different from the other four methods. It takes the view of a sensor model as describing the characteristics of the operating environment from the causes (occupancy) to the effects (measurements). This method was named forward model. This method uses the expectation maximization (EM) algorithm. Using this method, the most probable map in the high dimensional space is searched. Owing to the consideration of the dependency of the states of the OG cells, the maps generated through this method are more consistent and accurate. The paper also claims that accurate results can be obtained with better sensor models considering the physical phenomena in the sensors.

To compare the different methods of mapping, a bench-marking suite consisting of 4 quantitative techniques to evaluate OG maps is proposed in [22]. After evaluating the grid mapping methods ([25], [23], [11], [24] and [19]) based on the bench-marking suite, the results show that the Thrun's (2001) [19] method performs best compared to the other methods. Konoligie's method [25] is rated second followed by Moravec and Elfes (1985) [23] and Matthies and Elfes (1998)[24]. Thrun's method using neural network is rated worst among all the other methods.

2.2 Evaluation of OG Maps

To evaluate the performance of an OG mapping algorithm, the generated OG maps need to be analyzed. To analyze the map quality, the generated occupancy map is compared with a bench-mark map.

For analysis in a simulation environment, the bench-mark map is usually the ground truth (GT) map. In [22], the introduction of a bench-marking suite using a set of metrics helps in evaluating the various mapping algorithms. The various elements in the suite include

- A comparison using correlation function by conceptualizing the generated map as an image.
- A direct comparison of the maps on a cell by cell basis.
- Analyzing the map based on its usefulness to a robot. A generated map is required to plan paths for navigation. Therefore, to analyze the generated map, the ideal number of possible paths are calculated and the number of paths that are incomplete due to occupied cells in the generated map are determined. Finally, the false occupied cells can be obtained by comparing the paths.

In [14] and [20], a set of metrics are derived by constructing a confusion matrix for comparing binarized occupancy maps. The metrics include the true positive rate (TPR), false positive rate (FPR) and the overall error (OE). The TPR quantifies the tendency of an algorithm to accurately identify occupied cells. The FPR quantifies the tendency of an algorithm to incorrectly judge a cell as occupied and the OE is the ratio of total number of falsely classified cells to the total cells compared.

An evaluation method for the accuracy of automotive OGs is presented in [26]. One of the map quality measures chosen in [26] is the map score (MS) for comparing two maps represented in probability values. Another quality measure is the occupied cells ratio that is determined by the ratio of the occupied cells in the test map to the occupied cells in the GT map. Similarly, the empty cells ratio is calculated using the number of empty cells in the test map and the GT map.

In search of a bench-mark map, a novel patch map that approximates the full Bayesian solution is developed for comparing the maps generated from various OG mapping methods [27]. The maps generated from various OG mapping methods are compared with the bench-mark map using the Kullback-Leibler divergence metric. This metric quantifies how well one occupancy map resembles another.

2.3 Conclusion

The grid-based mapping methods provide a good framework for addressing the problem of constructing a map with known poses of the vehicle. Review on the relevant grid-based mapping methods show that there are predominantly two different methods for occupancy mapping. These are the inverse sensor model (ISM) based method and the forward sensor model (FSM) based method. In search of improvement to occupancy mapping, most of the other methods proposed in the literature modify the two basic methods. The inverse and forward models for occupancy mapping depends on the characteristics of the sensors. Furthermore, similar type of multiple sensors can contribute to the final occupancy map using grid fusion. In addition to the OG mapping methods, for investigating the performance of these methods, the comparison of the generated occupancy map with a bench-mark is necessary. Literature review on the evaluation of occupancy maps provides various possible metrics by which the comparison between a generated map and a GT map can be performed.

Chapter 3

Preliminaries

This chapter provides the mathematical basics used in occupancy mapping algorithms along with the fundamental concepts regarding ultrasonic sensors. Section 3.1 provides important concepts in probability with respect to occupancy mapping. In Section 3.2, concepts related to an ultrasonic sensor are presented. This section also explains how the occupancy information can be interpreted from an ultrasonic sensor measurement. Finally, Section 3.3 provides how an ultrasonic measurement can be synthesized at simulation level.

3.1 Basic Probability Concepts

This section provides the basic notations and important axioms of probability, which are further used in this thesis. In probabilistic mapping, quantities such as sensor measurements and states of the environment are modelled as random variables [28]. These random variables can take multiple values corresponding to the various states the quantities can attain. In addition, these variables obey the fundamental laws of probability. Let a random variable be denoted by X and x denote one of the possible events that is taken by this random variable. Then, the probability of the event x is represented as $p(X = x)$. If there are n discrete possible events, then the sum of all the probabilities of the individual outcomes for which the random variable X takes all possible values of x_j is one [29]. That is,

$$\sum_{j=1}^{n} p(X = x_j) = 1. \tag{3.1}$$

The probabilities are always non-negative, i.e., $p(X = x_j) \geq 0, \forall\, j \in \{1, \ldots, n\}$. Furthermore, in probabilistic mapping, the measurements and estimations are modeled for continuous spaces. These continuous spaces are characterized by random variables that can take continuum of values. These continuous random variables use functions to represent the probability for all the possible continuum of values. These functions are generally called probability density functions (PDFs). One of the common density functions in probabilistic mapping is a Gaussian/normal distribution with parameters mean and variance. This normal distribution is generally used to represent measurement noise in sensor measurements. This distribution is given by

$$p(x) = \left(\frac{1}{\sqrt{2\pi\sigma^2}}\right) \exp\left\{-\frac{1}{2}\frac{(x-\mu)^2}{\sigma^2}\right\}, \tag{3.2}$$

where σ^2 is the variance and μ is the mean of the distribution. Similar to discrete probability distribution, in continuous probability distribution, the integral over all probability values is 1 [28, 29]. That is,

$$\int_{-\infty}^{\infty} p(x)dx = 1. \tag{3.3}$$

Let x and y be two events from two dependent random variables X and Y. Then, the conditional probability [30] for the event x conditioned that the event y already took place is given by

$$p(x \mid y) = \frac{p(x)p(y)}{p(y)}. \tag{3.4}$$

In case the random variables X and Y are independent, then Y has no influence on X. Therefore, if the interest is on knowing X, then there is no advantage of knowing any information of Y [30]. This implies,

$$p(x \mid y) = \frac{p(x)p(y)}{p(y)} = p(x). \tag{3.5}$$

Another important and useful result of conditional probability is the Bayes rule [30], which relates conditionals of the type $p(x \mid y)$ to its inverse, $p(y \mid x)$. The rule is given as

$$p(x \mid y) = \frac{p(y \mid x)p(x)}{p(y)}. \tag{3.6}$$

If x is the quantity (e.g., position of the robot, map state) that needs to be inferred from the event y, then $p(x)$ is the prior probability distribution of the quantity x and y is the data (e.g., sensor measurement). The prior probability distribution is the previous knowledge on the quantity x without considering the new data y. The resultant probability $p(x \mid y)$ is the posterior probability distribution over X. The inverse probability $p(y \mid x)$ is often called the "generative model" as it describes how the variables of X cause the change in data Y. Finally, $p(y)$ in Bayes rule does not depend on x; hence the factor $p(y)^{-1}$ is same for any value x in the posterior $p(x \mid y)$.

The above-mentioned Bayes rule (3.6) can be extended if an arbitrary other variable is also considered, such as the variable Z. Then, the conditional probability of an event x from the random variable X conditioned that the events y and z from the variables Y and Z already took place is written as,

$$p(x \mid y, z) = \frac{p(y \mid x, z)p(x \mid z)}{p(y \mid z)}. \tag{3.7}$$

If the objective is to find the combined probability of the events x and y conditioned that the event z already took place, then the rule of combined probabilities can be used. The rule for combining

probabilities of the independent random variables X and Y conditioned on another variable Z is written as,

$$p(x, y \mid z) = p(x \mid z)p(y \mid z). \tag{3.8}$$

One of the important concepts in probability theory is that of the expectation of a random variable [30]. If X is a discrete random variable having a probability function $p(x)$, the expectation or the expected value of X, denoted by $E[X]$, is given by

$$E[X] = \sum_{j=1}^{n} x_j p(X = x_j). \tag{3.9}$$

The expected value of X is a weighted average of the possible values that X can take on, and each value being weighted by the probability of the corresponding individual outcomes. If X is a discrete random variable that takes on one of the values x_j, for $j \geq 1$, with respective probabilities, then for any real valued function $g(x)$

$$E[g(x)] = \sum_{j=1}^{n} g\left(x_j\right) p\left(x_j\right). \tag{3.10}$$

Another useful axiom in the concept of expectation involving constants is

$$E[aX + b] = aE[X] + b, \tag{3.11}$$

where a and b are constants.

The observation data of a random variable can be fit to a distribution function to estimate the probability of its events. This sampling distribution function could be parameterized by the observation data and other unobserved parameters. Maximum A Posterori (MAP) estimation of a random variable is obtained by knowing the parameters that maximizes the distribution function given that an event from a dependent random variable is observed. Therefore, the likelihood of an event of random variable occurring for the observed data could be obtained by determining the function (likelihood function) value for the given parameter. A MAP estimate is a straight forward method for known parameters from observation data; however, a few parameters could be hidden or unobserved from the data. Hence, the following paragraphs explain such a scenario related model and a method to determine the MAP estimate.

Hidden Markov model (HMM) is based on augmenting the Markov chain [31]. A Markov chain is a mathematical system that experiences transitions from one state to another according to certain probabilistic rules [32]. A Markov chain assumes that a transition to a particular state is solely dependent on the current state. In a hidden Markov model, the events of interest are either hidden or not observed directly. For example, if two coins (say "A" and "B") are tossed, the observations of the experiment show whether the tossed coin resulted in heads or tails. However, it is not known directly if the coin tossed was coin A or coin B. Therefore, if the event of interest is knowing the identity of the coin, then this is a hidden parameter as it is not known from the observation.

One of the solutions to solve the problem of estimating the parameters of a HMM is expectation-maximization (EM) algorithm. The EM algorithm is an iterative method to find the maximum likeli-

hood or maximum a posterior (MAP) estimates of parameters in a HMM. The EM algorithm generally consists of two steps [33]:

- E-step: Estimate the missing/latent variables with expected values.
- M-step: Calculation of a regular likelihood estimation using the expected values for the hidden parameter computed in the E step and values of the other variables.

The above-mentioned steps are iterated until convergence of the algorithm takes place.

3.2 Ultrasonic Sensor

Ultrasonic sensors are one of the proximity sensors used to obtain information of obstacles in the surrounding environment. These sensors emit sound waves using a transmitter and measure the time for the sound to bounce back to the receiver, also known as the time of flight [34]. In the state of art ultrasonic sensors, both the transmitter and the receiver are present in a single sensor unit. Using the time of flight and the velocity of the sound waves, the distance between the sensor and the target obstacle can be calculated. Hence, these sensors obtain the obstacle information by measuring the distance between the sensor position and the first obstacle reflecting the sound waves.

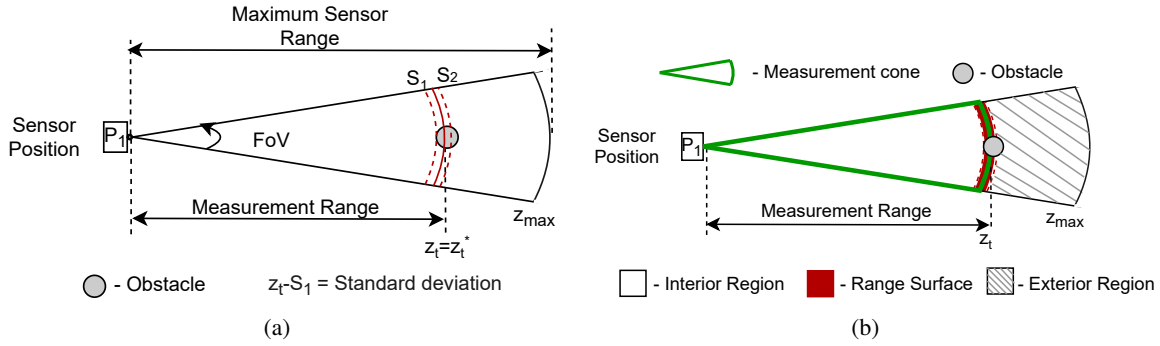

Figure 3.1: (a) Top view of a sensor cone showing a measurement and its noise variance, (b) Occupancy regions inferred based on an obtained measurement.

To understand the nomenclature related to an ultrasonic sensor, the top view of the sensor detecting an obstacle is shown in Figure 3.1a. The FoV of a sensor is the angle through which the sensor is sensitive to obstacles. The maximum range of the sensor is the distance limit up to which the sensor is able to detect an obstacle. The maximum range and the FoV angle specifies the sensitive area of an ultrasonic sensor. This sensitive field is also called the sensor cone. The measurement of an ultrasonic sensor provides information that an obstacle is present at a certain distance; however, there is no information on the angular position of the detected obstacle. This implies that the obstacle position can be estimated in the measurement arc spread over the field of view. This measurement arc is represented by a solid red line in the figure. Furthermore, a measurement cone is the virtual cone formed by the measurement range and the sensor FoV, as shown in Figure 3.1b.

Although the exact position of the obstacle cannot be inferred from the measurement, three important regions can be differentiated based on the measurement range arc [35]. These three regions inferred from the measurement are represented in Figure 3.1b. The first region is the region inside the measurement cone also called the interior region, which indicates that the area is free from obstacles. The second region is the region beyond the measurement range arc, where no information is available. The third region of measurement arc is also called the range surface, where the obstacle can be present anywhere on the arc.

One of the characteristics of an ultrasonic sensor is the sensitivity variation with respect to the spatial angle [36]. This sensitivity variation is directly associated to the beam pattern of the ultrasonic sensor, which is a 2D representation of the detection area of the sensor. This pattern is determined by factors such as the frequency of operation and the size, shape and acoustic phase characteristics of the vibrating surface. Therefore, in order to understand the sensitivity variation with respect to the spatial angle, the horizontal view pattern of the ultrasonic sensor can be experimentally determined. It is worth to mention here that the vertical view is not given priority as the height of the obstacle is not important for a 2-dimensional map. For ultrasonic sensors, targets beyond the beam angle (FoV) can be inadvertently detected. Therefore, considering the pattern obtained from the experiments, the chances of detecting an obstacle at a certain distance and an angular position can be modeled.

Another characteristic of an ultrasonic sensor is its sensitivity to angle of obstacle surface and the reflective properties of the surface. This sensitivity is associated to the phenomenon of specular reflection of the sound waves caused by different relative positions of the sensor and the reflecting surfaces of the obstacles. When sound waves emitted from the sensor do not get reflected back entirely upon hitting a surface sufficiently farther from the perpendicular axis, the phenomenon of specular reflection occurs [34]. Since a significant percentage of the sound waves do not reflect back to the sensor directly, the measurement observed tends to be at a longer distance than the ground truth distance. Therefore, this characteristic of the sensor leads to random measurements and should be given less priority consideration while mapping.

In addition to the random measurements caused by an ultrasonic sensor, the measurements can also be slightly deviated from the ground truth value. This deviation is present in any distance measuring sensor, and is also called measurement noise. In Figure 3.1a, let the true range of the object be denoted as z_t^*. In the scenario shown in the figure, the true range of the object is same as the measured range of the sensor, i.e., $z_t = z_t^*$. However, this is not always the case as the measurement can deviate from the true measurement. If the measurement is not affected by random phenomena, then the measurement is likely to fall in the region of $S_2 - S_1$. This deviation from the true value is due to measurement noise and can be represented as δ_t. Therefore, the measurement of an ultrasonic sensor with noise can be written as,

$$z_t = z_t^* + \delta_t. \tag{3.12}$$

In general the sensor noise is modeled as a Gaussian noise. Furthermore, based on the ultrasonic sensor nomenclature, a simple sensor model can be constructed for a non-random measurement from the sensor. A sensor model is a mathematical interpretation of the occupancy state of any point inside sensor cone given a sensor measurement. Let x be any point inside sensor cone. Then, its occupancy state is given by

$$O_x = \begin{cases} \text{Empty, if } d_x \leq S_1, \\ \text{Occupied, if } d_x > S_1 \text{ and } d_x < S_2, \\ \text{Not known, if } d_x \geq S_2, \end{cases} \tag{3.13}$$

where, O_x is the occupancy state of a point x. Here, d_x denotes the Euclidean distance of the point x

with respect to the sensor position. The radial distances S_1 and S_2 are dependent on the noise profile of the sensor.

3.3 Synthetic Sensor Data

For constructing an occupancy map, information of the surrounding environment is obtained using sensors. Ultrasonic sensors are used to perceive the surroundings of the ego-vehicle. Synthetic data of these ultrasonic sensors is required to implement and test occupancy mapping algorithms at simulation level. Therefore, the automated driving toolbox in MATLAB is used to replicate the scenario of a vehicle with sensors perceiving its surroundings. The surroundings of the vehicle are represented as grid cells. The grid cells in the vehicle's environment are represented as cost values, where a higher cost implies the presence of an obstacle.

Figure 3.2 shows an obstacle in the vehicle environment along with the vehicle itself. To obtain the sensor measurement synthetically, the sensor position and the sensor characteristics represented as sensor parameters need to be fixed. The sensor position is fixed at the mid-point of the vehicle's front side and the sensor parameters considered are:

- Sensor range: 2.5m,
- FoV angle : 40deg.

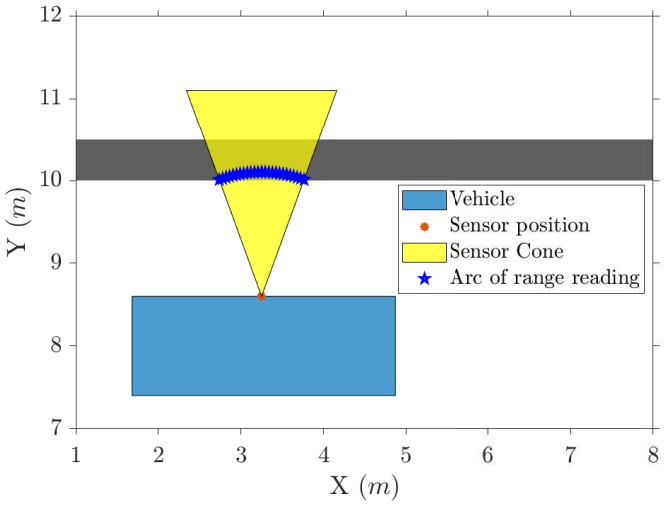

Figure 3.2: Representation of the physical environment along with the sensor cone to obtain synthetic sensor data.

Using the above sensor parameters, the sensor cone can be represented as shown in Figure 3.2. For synthetic sensor measurement, all cells inside the sensor cone are checked for the obstacle (i.e., cost value ≥ 0.9). If an obstacle is found in any point inside the sensor cone, then the Euclidean distance between the point and the sensor position is calculated. If multiple cells contain an obstacle inside

the sensor cone, then the minimum of all the calculated Euclidean distance is considered as the sensor measurement. On the other hand, if none of the cells contains an obstacle, then the maximum range is returned as the sensor measurement. It is worth to mention here that the sensor resolution is same as the resolution of the ground truth cost map created. Hence, true value of the distance between the sensor position and the obstacle is obtained as the measurement. The measurement value obtained is the ideal measurement without sensor noise, which is also not affected by random phenomenon.

The sensor data provides only the radial distance at which the obstacle is present and does not provide any angular information. This also means that the obstacle can be anywhere on the arc of sensor measurement. This is indicated in Figure 3.2 as the arc of range reading. Therefore, with only one sensor measurement, it is not possible to locate the obstacle's exact position.

3.4 Chapter Summary

In this chapter, in order to understand the occupancy grid mapping algorithms involving probability and statistics, the basic notations and axioms of probability are presented. Furthermore, the physical characteristics of the ultrasonic sensor influencing the mapping process are briefly described. These characteristics are responsible for the random and non-random measurements from ultrasonic sensors. Furthermore, based on the ultrasonic sensor nomenclature, a simple sensor model is constructed. The ideal ultrasonic sensor measurement is obtained by synthesizing the data at simulation level.

Chapter 4

Inverse and Forward Model-based Occupancy Grid Mapping

In this chapter the two different algorithms that are used predominantly for occupancy grid (OG) mapping are explained. The first method is based on the inverse sensor model (ISM) [17] for interpreting the sensor measurements to build the OG map. In this method of map building, a recursive update [11] is employed using the ISM to account for the new sensor measurements obtained at different instances. Therefore, Sections 4.1.1 and 4.1.2 explain the formulation of the ISM and the derivation of the recursive update respectively.

The second method for OG mapping, known as the forward sensor model (FSM) based mapping [19], approaches the mapping problem as a maximization of sensor measurement data likelihood given the various possible maps. The map that maximizes the sensor measurement data likelihood is chosen as the map closely representing the physical environment. This method of OG mapping considers most of the characteristics of the sensor measurements explained in the previous chapter. In Section 4.2.1, the background information for the sensor measurements is explained along with its prior probabilities. Subsequently, Section 4.2.2 describes the evidence-sensor model for interpreting the obtained sensor measurements. To complete the FSM and for solving the maximization problem, the expectation-maximization method is employed in Section 4.2.3. Finally, the framework of the FSM based mapping algorithm is elaborated in the Section 4.2.4.

4.1 Inverse Sensor Model-based OG Mapping

Inverse Sensor model-based mapping [11], also called the log-odds method, provides the occupancy information of the cells of the OG map falling inside the sensor cone based on the obtained sensor measurements. This occupancy information can be obtained by adhering to the regions of the sensor cone defined in the previous chapter. A mathematical model is required to represent occupancy information of the grid cells of the map. Each cell in the occupancy map can be identified using two parameters. The first parameter is the Euclidean distance between the sensor position and the cell. The other parameter is the angle made by the ray joining the cell and the sensor position with respect to the main vertical axis of the sensor cone. Therefore, the mathematical model should be a probability distribution as a function of the parameters of each cell in the occupancy map. Through this mathematical

model, each measurement of the sensor can be interpreted into occupancy information of the associated cells. However, to obtain a complete map of the environment, all the new sensor measurements obtained should be combined with the old. In addition, for areas with new measurements overlapping on the old measurements, the occupancy information needs to handled effectively by considering the new measurements as a new evidence. This combination of measurement data from multiple sensors to obtain coherent information of the environment is called sensor fusion. Therefore, the subsequent sections describe the sensor model followed by a method to fuse multiple sensor information.

4.1.1 Inverse Sensor Model

The Inverse sensor model is a probability distribution as a function of the cell parameters, which provides the occupancy information of the cells associated with a sensor measurement. In this thesis, an ideal sensor model is considered with the following assumptions.

- Conditional independence [27]: The occupancy of a cell is independent of its neighboring cells in the map. This independence implies that the cell occupancy is assigned without considering the occupancy of the other cells in the map.
- Uniform distribution of probability is considered inside the measurement cone.
- Uniform distribution of probability over all angles deviating from the main vertical axis inside the field of view of the sensor.
- Measurement aberrations are not considered.

Considering the above assumptions, the sensor model interpreting a sensor measurement to represent the occupancy of the cells falling inside the measurement cone is framed as

$$p\left(m_{x,y} \mid z\right) = \begin{cases} p_{emp}, \text{ if } d_{x,y} < z \text{ and } 2\theta_{x,y} < \theta_{\text{FoV}} \\ p_{occ}, \text{ if } d_{x,y} = z \text{ and } 2\theta_{x,y} < \theta_{\text{FoV}} \\ 0.5, \quad \text{if } d_{x,y} > z \text{ or } 2\theta_{x,y} > \theta_{\text{FoV}} \end{cases}, \forall z \leq z_{\max}, \tag{4.1}$$

where m denotes a cell from the OG map with x and y representing the indices of a grid cell. The observation of a sensor, with a max-range value of z_{max}, at a given instance is denoted by z. In addition, the field of view angle of the sensor is represented by θ_{FoV}. The probabilities assigned for empty and occupied region based on the sensor measurement is p_{emp} and p_{occ}. The probability distribution is a function of the Euclidean distance between the cell considered and the sensor position. This Euclidean distance is denoted by $d_{x,y}$ and the angle made by the ray joining the cell and the sensor position with respect to the main vertical axis of the sensor cone is written as $\theta_{x,y}$. The probability distribution function results in the probability of the considered cell being occupied for the given sensor measurement.

Although (4.1) provides the occupancy information of cells for a single ultrasonic sensor measurement, the information from all the ultrasonic sensors around the vehicle needs to be fused for complete knowledge of the vehicle's surrounding environment. Therefore, interpretation of the information needs to be extended to multiple observations using an appropriate update method. This update method employs the Bayes rule, which is stated in Chapter 3, and this is explained in the further section.

4.1.2 Log-odds Update

A map update is crucial for ascertaining whether a cell is empty or occupied and to obtain a complete map of the surrounding. The update is crucial because each sensor measurement provides only partial evidence of a cell being occupied or empty [17]. This uncertainty is due to unavailability of the exact angular information of the obstacle detected. Therefore, the ascertainment could be provided by interpreting information from multiple sensors over multiple poses. The log-odds update method using the Bayes rule updates the existing map using the new measurement taking into account the old measurements.

To derive the recursive update equation, the problem of map occupancy probability for various sensor observations obtained is mathematically formulated as, $p\left(M|z_1, \ldots, z_T\right)$. The parameter z_i denotes a single ultrasonic sensor measurement obtained at various time steps. The time steps are denoted by subscript i, i.e., from 1 to T. The entire occupancy grid map is denoted by M and its each component cell is denoted by $m_{x,y}$. Here, x and y are the indices of the cell. Based on the assumption that each cell's occupancy is independent of its neighboring cell's occupancy, the map occupancy probability can be calculated for individual cells. Applying Bayes rule to the occupancy probability for each map cell $m_{x,y}$ considering the obtained sensor measurements, we have

$$p\left(m_{x,y} \mid z_1, \ldots, z_T\right) = \frac{p\left(z_T \mid m_{x,y}\right) p\left(m_{x,y} \mid z_1, \ldots, z_{T-1}\right)}{p\left(z_T \mid z_1, \ldots, z_{T-1}\right)}. \tag{4.2}$$

In the above equation, the term $p\left(m_{x,y} \mid z_1, \ldots, z_{T-1}\right)$ is the prior of the cell occupancy probability. This prior probability is also called the belief of occupancy. The term $p\left(z_T \mid m_{x,y}\right)$ is the likelihood of the new measurement z_T given the occupancy of the map cell $m_{x,y}$. The denominator in the equation is the marginal likelihood of the sensor measurement, which is the likelihood of the sensor measurement for all possible events. The ratio of the new sensor measurement likelihood to the marginal likelihood term is the support provided by the new sensor measurement to the prior occupancy probability.

Applying Bayes rule again to the term $p\left(z_T \mid m_{x,y}\right)$,

$$p\left(z_T \mid m_{x,y}\right) = \frac{p\left(m_{x,y} \mid z_T\right) p\left(z_T\right)}{p\left(m_{x,y}\right)}. \tag{4.3}$$

The term $p\left(m_{x,y} \mid z_T\right)$ is the sensor model, which was discussed in the previous section. Also, the term $p\left(m_{x,y}\right)$ is the probability of the map cell being occupied. Therefore, using (4.3), (4.2) becomes

$$p\left(m_{x,y} \mid z_1, \ldots, z_T\right) = \frac{p\left(m_{x,y} \mid z_T\right) p\left(z_T\right) p\left(m_{x,y} \mid z_1, \ldots, z_{T-1}\right)}{p\left(m_{x,y}\right) p\left(z_T \mid z_1, \ldots, z_{T-1}\right)}. \tag{4.4}$$

To obtain the map occupancy probability for all given sensor measurements, (4.4) should be solved. However, the probability of the sensor measurement being observed ($p(z_T)$) and the marginal probability terms are not easy to determine. Therefore, to eliminate these terms, the log-odds ratio is introduced. The log-odds of a state is defined as natural logarithm of the ratio of its probability (p) to its complementary probability ($1 - p$). For the probability of the map cell being occupied considering the obtained sensor measurements, the log-odds ratio is calculated as

$$l\left(m_{x,y} \mid z_1, \ldots, z_T\right) = \log \frac{p\left(m_{x,y} \mid z_1, \ldots, z_T\right)}{1 - p\left(m_{x,y} \mid z_1, \ldots, z_T\right)}. \tag{4.5}$$

The log-odds ratio $l\left(m_{x,y} \mid z_1, \ldots, z_T\right)$ can be written in short as $l_{x,y}^T$. Also, the log-odds can be converted back to the map cell probability by:

$$p\left(m_{x,y} \mid z_1, \ldots, z_T\right) = 1 - \left(1 + e^{l_{x,y}^T}\right)^{-1}. \tag{4.6}$$

Similar to (4.4), the negation of the probability of the map cell being occupied is the map freeness and denoted by $\bar{m}_{x,y}$. The probability for the freeness map cell is

$$p\left(\bar{m}_{x,y} \mid z_1, \ldots, z_T\right) = \frac{p\left(\bar{m}_{x,y} \mid z_T\right) p\left(z_T\right) p\left(\bar{m}_{x,y} \mid z_1, \ldots, z_{T-1}\right)}{p\left(\bar{m}_{x,y}\right) p\left(z_T \mid z_1, \ldots, z_{T-1}\right)}. \tag{4.7}$$

Using (4.4), (4.5) and (4.7) the log-odds recursive equation is formulated as,

$$l_{x,y}^T = \log \frac{p\left(m_{x,y} \mid z_T\right)}{1 - p\left(m_{x,y} \mid z_T\right)} + l_{x,y}^{T-1} - l_{x,y}^0, \tag{4.8}$$

where $l_{x,y}^0$ is the initial log-odds value given by

$$l_{x,y}^0 = \frac{p\left(m_{x,y}\right)}{1 - p\left(m_{x,y}\right)}. \tag{4.9}$$

4.1.3 Implementation

To implement the inverse sensor model (ISM) based mapping, the occupied and empty probabilities in (4.1) need to be set. Various values for p_{occ} and p_{emp} have been used in OG mapping literature [37, 38, 27]. These values depend on the sensor characteristics, and provide insights on the confidence of freeness/occupancy of a particular cell based on the sensor measurement. The values $p_{occ} = 0.8$ and $p_{emp} = 0.2$ reported in [27] are considered in this thesis. Figure 4.1 represents the probability distribution for a sensor measurement z_t with the sensor maximum range z_{max}. A low occupancy probability value is assigned for the cells at distance between 0 and the neighborhood of the measurement. The cells at distance of sensor measurement z_t are assigned a high probability value. Beyond the distance of z_t, the cells have an uncertain probability corresponding to the value 0.5.

The next step is to implement the sensor model and the recurring update equation discussed in Sections 4.1.1 and 4.1.2. The algorithm is split into three parts. The first part is the map initialization that assigns all the initial map occupancy probabilities as 0.5 (uncertain). In addition, these initial map probabilities are converted into log-odds form as in (4.9). In the second part, for all time instants, the log-odds update is carried out for the cells falling inside the sensor cone of the corresponding measurement. Finally, once the log-odds are computed for all grid cells, the log-odds form is converted back to map probabilities using (4.6) in the third part of the algorithm. This framework is put into an algorithm and is presented in Algorithm 4.1.

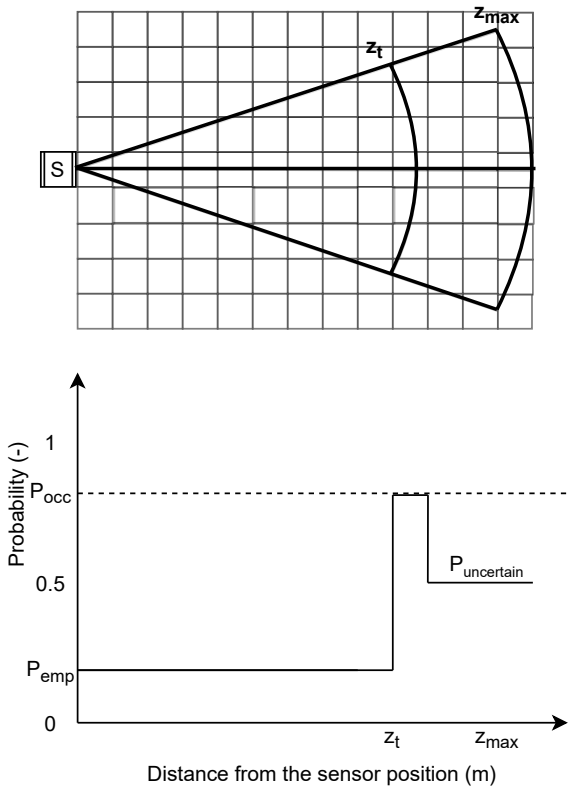

Figure 4.1: Inverse sensor model: The occupancy probabilities assigned for the OG map cells with respect to the distance of these cells from the sensor position.

Algorithm 4.1: ISM based mapping for single sensor

%% Initialization

for `all grid cells` **do**

$m^0_{x,y} = 0.5$

$l^0_{x,y} = \log \frac{m_{x,y}}{1-m_{x,y}}$

end

%% Update

for `all measurements` t `from time instants` 1 `to` T **do**

for `all grid cells` (x, y) `falling in the measurement cone of` t **do**

$l^t_{x,y} = \log \frac{p(m_{x,y}|z_t)}{1-p(m_{x,y}|z_t)} + l^{t-1}_{x,y} - l^0_{x,y}$

end

.

end

%% Obtain probabilities from log-odds

for `all grid cells` (x, y) **do**

$m_{x,y} = 1 - \left(1 + e^{l^T_{x,y}}\right)^{-1}$

end

Algorithm 4.1 is for obtaining the occupancy map for a single sensor providing measurements at various time instants. The implementation of the algorithm for a single sensor providing measurements at multiple time instants is illustrated with an example in Figures 4.2a and 4.2b. Figure 4.2a shows the ground truth map with the obstacles shown in black and the markers representing the location of the sensor. The OG map generated is shown in Figure 4.2b. In this figure, the lighter the color of a cell, lower the probability of the cell being occupied.

Algorithm 4.1 is extended for multiple sensors providing measurements at multiple time instants by grid fusion and is written in Algorithm 4.2. The posterior probability of the occupancy grid map cell for n number of sensors and for time instances 1 to T is denoted as $p(m_{x,y}|z_1^{1:n}, \ldots, z_T^{1:n})$. The log-odds ratio is represented in short as $l_{x,y}^{s,t}$ for a grid cell with indices x, y, where s and t denote the sensor and the time instance.

Algorithm 4.2: ISM based mapping for multiple sensors

%% Initialization
for *all grid cells* **do**
  $m_{x,y}^0 = 0.5$
  $l_{x,y}^0 = \log \frac{m_{x,y}}{1-m_{x,y}}$
end
%% Update
for *all measurements* t *from time instants* 1 *to* T **do**
  for *all sensors* s *from* 1 *to* n **do**
    for *all grid cells* (x, y) *falling in the measurement cone of* t **do**
      $l_{x,y}^{s,t} = \log \frac{p(m_{x,y}|z_t^s)}{1-p(m_{x,y}|z_t^s)} + l_{x,y}^{s-1,t} - l_{x,y}^0$
    end
    .
  end
end
%% Obtain probabilities from log-odds
for *all grid cells* (x, y) **do**
  $m_{x,y} = 1 - \left(1 + e^{l_{x,y}^{n,T}}\right)^{-1}$
end

To conclude, this section explained the ISM based mapping that interprets sensor measurements to obtain occupancy information of the surrounding environment. In [19], an alternative approach to generate occupancy map is presented. The alternative approach is used as the basis for this thesis to generate accurate occupancy grid maps considering all the major characteristics of the ultrasonic sensor (Chapter 3).

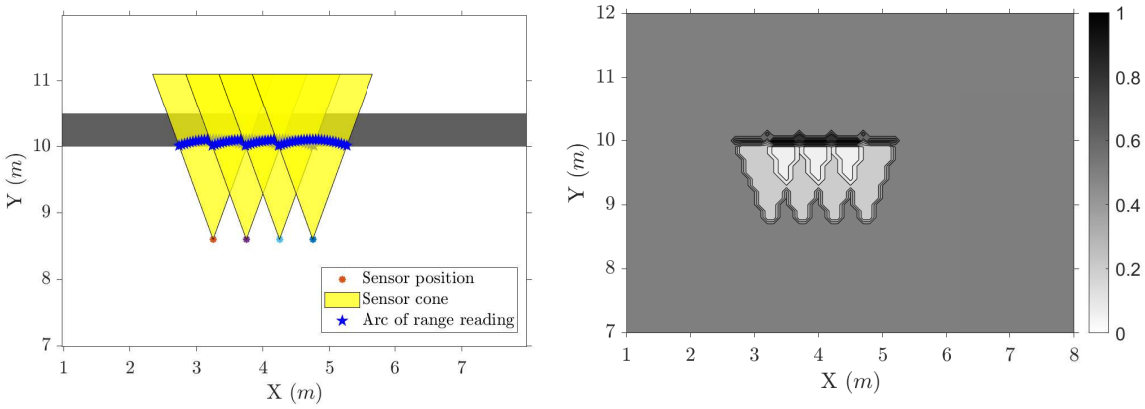

(a) (b)

Figure 4.2: (a) Ground truth environment and sensor cones, (b) OG map generated using the ISM-based algorithm.

4.2 Forward Sensor Model-Based OG Mapping

In forward sensor model (FSM) based OG mapping, the likelihoods of the observed sensor measurements for various possible maps are determined. Thereafter, the map which maximizes the observed sensor measurements likelihood is considered the most appropriate map. This model of mapping as a likelihood of the sensor measurements is represented as $p(Z|m)$. The parameter 'Z' is the set of all sensor measurements obtained at various time instances and 'm' is the OG map. It is worth to mention here that the vehicle poses corresponding to the sensor measurements are always available, and hence not considered in any of the model representations.

One of the important assumptions made in the inverse sensor model (ISM) is to neglect the inter-cell dependencies which could assign higher occupancy value on all cells falling on range surface. However, the forward sensor model (FSM) considers the inter-cell dependency and considers the obstacle somewhere on the range surface and not everywhere. Another disadvantage of the ISM is that the random measurements of the ultrasonic sensor are not accounted in the model; however, this characteristic is also considered in the FSM for better interpretation of sensor measurements. Therefore, in the FSM, the two main measurement classes, random and non-random are accounted. Furthermore, the non-random measurements can also be combined with some measurement noise. The further section sets up the description of the FSM for incorporating the sensor characteristics in occupancy mapping.

4.2.1 Description of the FSM

As discussed in the previous section, an ultrasonic sensor measurement can imply two distinct events, the random phenomenon and detecting an obstacle. Apart from these events, an ultrasonic sensor measurement could also be at the max-range value. From experiments conducted in [39], it was observed that most of the max-range measurements were caused by the random phenomena and not because of any obstacle. Therefore, instead of considering the max-range measurements as a particular

case of non-random class (as in [19]), it is considered as a separate event. To sum up, for a given ultrasonic sensor measurement, three distinct events are possible and the prior probabilities for these events can be assigned. First, for the random measurements, the prior probability of obtaining a measurement from this kind of event is p_{rand}. Second, for the special case of random max-range values, the prior probability of obtaining this outcome is p_{max}. Finally, the non-random measurements are caused by the obstacles in the field of view of the ultrasonic sensor. The prior probability of the non-random measuring event is the remaining odds after the random event and the event of obtaining a max-range value, i.e., $1 - p_{rand} - p_{max}$. These prior probabilities are usually found empirically rather than assigning based on theoretical models.

Out of the three events, the non-random class measurements are the most informative as they signify the presence of an obstacle in the sensor field of view. To understand the prior distribution for a non-random measurement, lets consider three obstacles possibly causing the measurement. Also, let the event of an occupied cell reflecting the sonar beam have a probability of p_{hit}. An ideal ultrasonic sensor detects the first closest obstacle in the sensor cone, which implies that the probability of the first closest obstacle reflecting the sonar beam is 1. If the sonar beam is not reflected by the first obstacle, then this event has a negation of p_{hit}. Therefore, the probability of the second obstacle reflecting the sonar beam will be the combined probabilities of the events of obtaining a non-random measurement and overlooking the first closest obstacle, which is given as,

$$p(\text{non-rand}, \bar{H}_1, H_2) = (1 - p_{rand} - p_{max})(1 - p_{hit})p_{hit}. \tag{4.10}$$

Here, H_k represents the event of the k^{th} obstacle reflecting the sonar beam and $\bar{H}_k$ denotes the event of the k^{th} obstacle being overlooked by the sensor. Similar to (4.10), if the obstacle overlooks the first and second closest obstacles, then

$$\begin{aligned} p(\text{non-rand}, \bar{H}_1, \bar{H}_2, H_3) &= (1 - p_{rand} - p_{max})(1 - p_{hit})(1 - p_{hit})p_{hit}, \\ &= (1 - p_{rand} - p_{max})(1 - p_{hit})^j p_{hit}. \end{aligned} \tag{4.11}$$

The above equation is similar to a geometric distribution with parameter p_{hit}. The parameter j denotes the number of obstacles overlooked by the sensor. Therefore, each obstacle can be assigned a prior probability distribution as a function of p_{hit} and j. By providing radial distance as the priority for the obstacle numbering, the parameter j can be determined using $j = s_k - 1$, where s_k is the stance of the k^{th} obstacle. All the possible causes of a sensor measurement for the scenario of three obstacles in the sensor cone are shown in Figure 4.3. In addition to probability distribution based on the radial position as in [19], an angular probability distribution can also be incorporated to the prior of non-random class measurements.

To model an angular probability distribution (p_{ang}), it is important to analyze the horizontal view of the sensor over the angular FoV. Experiments conducted in [7] presented the horizontal view of the sensor over various angles in the sensor FoV, also shown in Figure 4.4a. It is clear from the figure that from approximately $-50deg$ to $+50deg$, the sensor has a range close to max-range value. However, for angles closer to horizontal plane, the range values increase gradually until $-50deg$ and $+50deg$ field of view. Therefore, the probability distribution could be modeled as a trapezoid with the short base denoting the highest probability values being maintained between $-50deg$ to $+50deg$ FoV and the sides of the trapezoid modeled for angles closer the horizontal plane, as shown in Figure 4.4b. The complete implementation of the trapezoidal distribution is presented in Appendix A.

In order to formally define the set of prior probabilities, the important denotations are described. Let z_t denote a single sensor measurement at time t. The sensor cone belonging to the measurement z_t

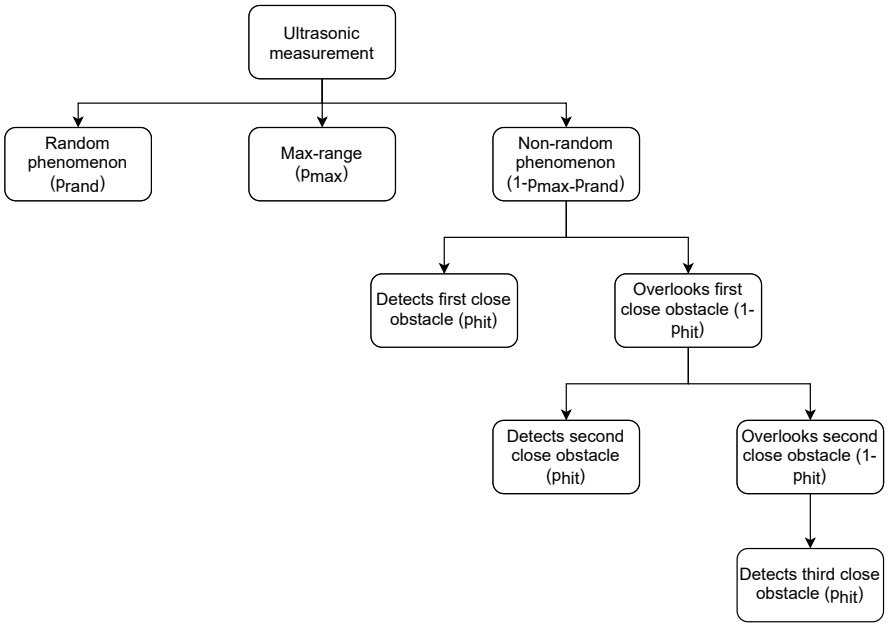

Figure 4.3: Flow chart showing various possible causes of an ultrasonic sensor measurement.

can be translated to the OG map. Let K_t be the total number of occupied cells in the OG map inside the sensor cone belonging to z_t. The radial distances of these occupied cells from the sensor position can be determined using the OG map and is written as

$$D_t = \{d_{t,1}, d_{t,2}, \ldots, d_{t,K_t}\} \tag{4.12}$$

with the distances sorted in increasing order, i.e.,

$$d_{t,1} \leq \ d_{t,2} \leq \ \ldots \leq d_{t,K_t}. \tag{4.13}$$

Since an obstacle can be anywhere on the arc of sensor measurement, a new set of variables is introduced corresponding to each occupied cell for describing the possible cause of a sensor measurement. These variables are called correspondence variables and are denoted as

$$c_t = \{c_{t,1}, c_{t,2}, \ldots, c_{t,K_t}\}. \tag{4.14}$$

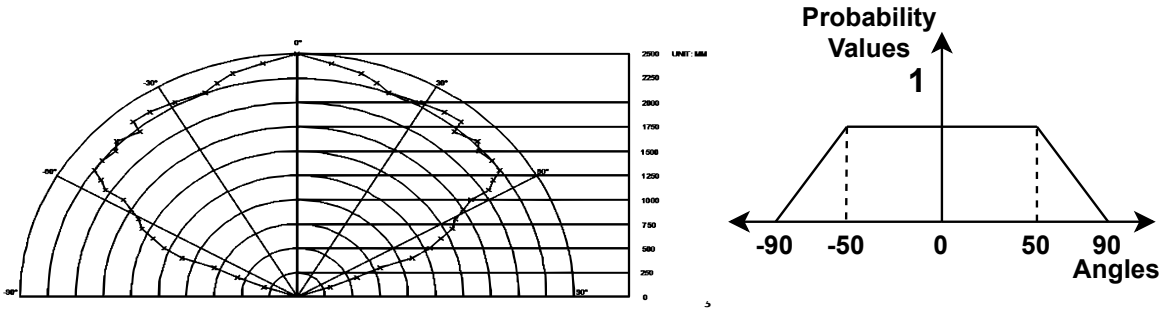

(a) (b)

Figure 4.4: (a) Horizontal field of view of an ultrasonic sensor [7], (b) Trapezoidal probability distribution modeled according to the horizontal field of view of the ultrasonic sensor.

In addition to the correspondence variables describing the cause of measurement as non-random, two more correspondence variables are included to describe the other two distinct events, i.e., obtaining random ($c_{t,*}$) and max-range values ($c_{t,0}$). Therefore, the complete set of correspondence variables is given as

$$c_t = \{c_{t,*}, c_{t,0}, c_{t,1}, c_{t,2}, \ldots, c_{t,K_t}\}. \tag{4.15}$$

All the correspondence variables are binary and provide the one cause of measurement. As a result, the correspondence variables are subject to the constraint

$$c_{t,*} + \sum_{k=0}^{K_t} c_{t,k} = 1. \tag{4.16}$$

For example, if $c_{t,k}$ is 1 for $1 \leq k \leq K_t$, then the cause of the measurement is from the k^{th} obstacle.

Now, the prior probabilities for all the possible causes of an ultrasonic sensors are summed up as

$$p(c_t) = \begin{cases} p_{\text{rand}}, \text{ if } c_{t,*} = 1, \\ p_{\text{max}}, \text{ if } c_{t,0} = 1, \\ (1 - p_{\text{rand}} - p_{\text{max}})(1 - p_{\text{hit}})^{s_k - 1} p_{\text{hit}} p_{\text{ang}}, \text{ if } c_{t,k} = 1, \text{ for } 1 \leq k \leq K_t. \end{cases} \tag{4.17}$$

The parameter s_k in the geometric distribution denotes the stance of the k^{th} occupied cell in the sensor cone. This stance numbering starts for the occupied cells closest to the sensor with 0. Furthermore, if multiple occupied cells are at a same radial distance from the sensor position, then all these cells are given equal priority in the positioning number.

This section described the basic set up to account the various sensor measurement classes and interpreted the background information of the sensor as prior probabilities. The next section will explain the evidence (measurement) given that the background information is known.

4.2.2 Evidence – Sensor Model

The evidence-sensor model provides the probability distribution based on the new sensor measurement given that the cause of measurement in known. For a random cause, the measurement can be anywhere over the sensor range, i.e., from 0 to max-range. Hence a uniform probability distribution is modeled over the defined sensor range and otherwise the probability is 0.

$$p(z_t \mid m, c_{t,*} = 1) = \begin{cases} \frac{1}{z_{\text{max}}}, \text{ if } 0 \leq z_t < z_{\text{max}}, \\ 0, \text{ otherwise.} \end{cases} \tag{4.18}$$

For the special case of random measurement being equal to the max-range value, a Gaussian distribution centered on z_{max} is modeled with noise variance σ^2 :

$$p(z_t \mid m, c_{t,0} = 1) = \begin{cases} \frac{1}{\sqrt{2\pi\sigma^2}} e^{-\frac{(z_t - z_{max})}{2\sigma^2}}, \text{ if } z_t = z_{max}, \\ 0, \text{ otherwise.} \end{cases} \tag{4.19}$$

For a non-random measurement reflected by an obstacle k at distance $d_{t,k}$, the measurement noise is modeled as a Gaussian centered at the distance $d_{t,k}$ with noise variance σ^2.

$$p\left(z_t \mid m, c_{t,k}=1\right)=\begin{cases} \frac{1}{\sqrt{2\pi\sigma^2}} e^{-\frac{\left(z_t-d_{t,k}\right)}{2\sigma^2}}, \text{ if } 0 \leq z_t < z_{max}, \\ 0, \text{ otherwise.} \end{cases} \tag{4.20}$$

The complete sensor model over all correspondence variables can be obtained by merging the above equations (4.18), (4.19), (4.20). According to (4.16), only one correspondence variable can take value 1 for a sensor measurement. Also, to combine the probabilities, the distribution functions are multiplied. Therefore, to bring in the dependency of the correspondence variable, the respective variables are raised to the power of their functions.

$$p\left(z_t \mid m, c_t\right)=\left(\frac{1}{z_{max}}\right)^{c_{t,*}} \frac{1}{\sqrt{2\pi\sigma^2}} e^{\frac{(z_t-z_{max})c_{t,0}}{2\sigma^2}} \prod_{k=1}^{K_t} \frac{1}{\sqrt{2\pi\sigma^2}} e^{-\frac{\left(z_t-d_{t,k}\right)c_{t,k}}{2\sigma^2}}. \tag{4.21}$$

With the knowledge of the prior probability based on the background information and the evidence-sensor model, the joint probability distribution of the sensor measurement for a given map can be determined.

4.2.3 Calculating Posterior for all Sensor Data

Posterior probability is the probability of an event occurring, which is determined by considering the new evidence and the background information (prior). On the other hand, prior is the probability an event occurs without considering the new evidence. Therefore, the posterior probability distribution combines the prior distribution and the information from a new evidence (observation). That is,

$$p(z_t, c_t|m) = p(c_t)p(z_t|m, c_t), \tag{4.22}$$

where the right hand side terms represent the prior and the evidence discussed in the previous sections. The previous models were derived for a single sensor measurement z_t. For all time instances of a single sensor, the combined probability is the product of probabilities at each time instance, i.e.,

$$p(Z, C|m) = \prod_t p\left(z_t, c_t|m\right), \tag{4.23}$$

where 'Z' denotes the set of all the measurements and 'C' denotes the set of all correspondences for all data. In statistics, the log likelihood is calculated in order to reduce computational complexity of values close to zero. Therefore, equation (4.23) becomes

$$\log p(Z, C|m) = \sum_t \log p\left(z_t, c_t|m\right). \tag{4.24}$$

Since the set of correspondence variables are not observed, the posterior of the correspondence variables are determined by calculating the expectation of the log-likelihood over all the correspondence

variables. Therefore, the expectation of (4.24) is

$$\begin{aligned} E[\log p(Z,C|m)|Z,m] &= E\left\{\sum_t \log\left(p\left(z_t|c_t,m\right)p\left(c_t\right)\right)|Z,m\right\}, \\ &= \sum_t [E\left[\log p(c_t)\right]|Z,m + E\left[c_{t,*}|z_t,m\right]\log p\left(z_t|m,c_{t,*}=1\right) \\ &\quad + E\left[c_{t,0}|z_t,m\right]\log p\left(z_t|m,c_{t,0}=1\right) \\ &\quad + \sum_{k=1}^{K_t} E\left[c_{t,k}|z_t,m\right]\log p\left(z_t|m,c_{t,k}=1\right)], \end{aligned} \tag{4.25}$$

where z_t denotes a single sensor measurement at time t, K_t is the total number of obstacles in the sensor cone $z_t$and c_t denotes the set of correspondence variables. (4.25) provides the log-likelihood for the measurements over all time instants. Maximizing this log-likelihood will provide the most likely map for the observed sensor measurements. For maximizing the above function, the posterior probability of the correspondence variable is required. This probability is also called the expectation term.

The correspondence variable is not observed through the sensor measurements. Therefore, this variable is also called the latent variable. The problem of maximizing the log-likelihood is now based on two parameters, i.e., 'z' and 'c', where 'z' is the observed parameter and 'c' is the latent variable. This type of problem where it is important to find the latent variable/unobserved parameter for determining the most likely map through a maximization process is solved with the help of the expectation-maximization (EM) algorithm.

In the EM algorithm, the log-likelihood is calculated for a predetermined correspondence value (posterior probability) through the expectation step. In the maximization step, the log-likelihood is maximized, and its corresponding parameters are chosen. The following sections explain the mathematics behind the expectation step and the maximization step for the current problem of occupancy mapping. Furthermore, after the E and M step derivation, the occupancy map algorithm using the EM steps are explained.

Calculating Expectations (E-step)

This step calculates the expectation of each correspondence variables for a given map m and sensor measurement z_t. Since the correspondence variables are Bernoulli variables (taking values 0 or 1) the expected value is the probability itself. Therefore,

$$E\left[c_{t,*}=1|z_t,m\right] = p(c_{t,*}=1|m,z_t). \tag{4.26}$$

In order to determine the above probability, first, the joint probability of the correspondence variable and the measurement is written as,

$$p(c_{t,*}=1,z_t|m) = p(c_{t,*}=1|m,z_t)p(z_t). \tag{4.27}$$

Using (4.23) in the above equation to substitute the term $p(c_{t,*}=1,z_t|m)$, the above equation becomes,

$$p(z_t|m,c_{t,*}=1)p(c_{t,*}=1) = p(c_{t,*}=1|m,z_t)p(z_t).$$

The probability of the latent variable is to be determined. Therefore, the above equation is rearranged as

$$p(c_{t,*} = 1|m, z_t) = \frac{p(z_t|m, c_{t,*} = 1)p(c_{t,*} = 1)}{p(z_t)}. \tag{4.28}$$

Using (4.18) and (4.17) in the above equation,

$$\begin{aligned} p(c_{t,*} = 1|m, z_t) &= \frac{1}{p(z_t)} \frac{1}{z_{max}} p_{rand}, \\ &= \eta \frac{1}{z_{max}} p_{rand} = e_{t,*}, \end{aligned} \tag{4.29}$$

where η is the normalization constant.

Similar to $e_{t,*}$, the expectation for max-range ($e_{t,0}$) and non-random ($e_{t,k}$) cases can be determined.

$$\begin{aligned} E\left[c_{t,0} = 1|z_t, m\right] &= p(c_{t,0} = 1|m, z_t), \\ &= \frac{p\left(z_t|m, c_{t,0} = 1\right) p\left(c_{t,0} = 1|m\right)}{p(z_t|m)}, \\ &= \frac{p\left(z_t|m, c_{t,0} = 1\right) p_{rand}}{p(z_t|m)}, \\ &= \eta \frac{1}{\sqrt{2\pi\sigma^2}} e^{-\frac{(z_t - z_{max})}{2\sigma^2}} . p_{max} = e_{t,0}. \end{aligned} \tag{4.30}$$

$$\begin{aligned} E\left[c_{t,k} = 1|z_t, m\right] &= p(c_{t,k} = 1|m, z_t), \\ &= \frac{p\left(z_t|m, c_{t,k} = 1\right) p\left(c_{t,k} = 1|m\right)}{p(z_t|m)}, \\ &= \frac{p\left(z_t|m, c_{t,k} = 1\right) (1 - p_{hit})^{s_k - 1} . p_{hit} p_{ang}}{p(z_t|m)}, \\ &= \eta p\left(z_t|m, c_{t,k} = 1\right) (1 - p_{rand} - p_{max})(1 - p_{hit})^{s_k - 1} p_{hit} p_{ang}, \\ &= \eta \frac{1}{\sqrt{2\pi\sigma^2}} e^{\frac{\left(z_t - d_{t,k}\right)}{2\sigma^2}} (1 - p_{rand} - p_{max})(1 - p_{hit})^{s_k - 1} p_{hit} p_{ang} = e_{t,k}. \end{aligned} \tag{4.31}$$

Using (4.29), (4.30) and (4.31), the normalization constant η can be calculated as

$$\eta = \left(\frac{1}{z_{max}} p_{rand} + \frac{1}{\sqrt{2\pi\sigma^2}} e^{-\frac{(z_t - z_{max})}{2\sigma^2}} p_{max} \right. \tag{4.32}$$

$$\left. + \frac{1}{\sqrt{2\pi\sigma^2}} e^{\frac{\left(z_t - d_{t,k}\right)}{2\sigma^2}} (1 - p_{rand} - p_{max})(1 - p_{hit})^{s_k - 1} p_{hit} p_{ang} \right)^{-1}. \tag{4.33}$$

Maximization step (M-step)

The expectation functions calculated in the previous section are used in the maximization function to evaluate the likelihood of all sensor measurements for the various possible maps. Finally, the map

which maximizes the expected log-likelihood will be most likely map for the given set of measurements. The maximization function is determined by incorporating the expectation functions in the log-likelihood derived in Section 4.2.3. Therefore, Equation (4.25) becomes

$$E[\log p(Z,C|m)|Z,m] = \sum_t \Bigg[E\left[\log p(c_t)\right]|Z,m + e_{t,*} \log p\left(z_t|m,c_{t,*}=1\right) + e_{t,0} \log p\left(z_t|m,c_{t,0}=1\right) + \sum_{k=1}^{K_t} e_{t,k} \log p\left(z_t|m,c_{t,k}=1\right) \Bigg]. \quad (4.34)$$

From the above equation, the overall probability of the correspondences do not change with various sensor measurements. Therefore, the first term can be neglected and (4.34) becomes

$$E[\log p(Z,C|m)|Z,m] = \sum_t \Bigg[e_{t,*} \log p\left(z_t|m,c_{t,*}=1\right) + e_{t,0} \log p\left(z_t|m,c_{t,0}=1\right) + \sum_{k=1}^{K_t} e_{t,k} \log p\left(z_t|m,c_{t,k}=1\right) \Bigg]. \quad (4.35)$$

4.2.4 Implementation

Algorithm 4.3 shows the forward sensor model based mapping algorithm that is split into two main parts. The first part is the initialization that sets the initial map as completely unoccupied, i.e., all grid cells occupancy as zero. Although the initialization could be different rather than keeping the complete map unoccupied, it was found empirically in [19] that the convergence speed was faster for a completely unoccupied initial map. Since this algorithm generates an occupancy map for a batch of sensor measurements, all the sensor measurements obtained from multiple sensors at multiple time instances are grouped in a vector of size N. The next main step is the EM optimization; this step can be broken down into the E-step and the M-step. In the E-step, the expectation terms for the log-likelihood calculation in the M-step are determined. In the M-step, the maximization function, i.e., the log-likelihood for all the sensor measurements are calculated for a given map.

For implementing the E-step to determine expectation terms, equations (4.29), (4.30), (4.31) are computed along with (4.33) for the random and the non-random cases. In the non-random case, before computing (4.31), the distances of the occupied cells are determined for the given map. Various maps in the maximization are iterated by setting temporarily the selected cell $< x, y >$ to occupied (i.e., $i = 1$). Initially the log-likelihood function is computed for the map with cell $< x, y >$ considered not occupied. Thereafter, the occupancy of the considered cell is set to occupied and the expectations for the map with cell $< x, y >$ being occupied is recalculated. Similarly, the log-likelihood for this case is also recalculated. Finally, the log-likelihoods for the map with cell $< x, y >$ occupied and map with the same cell not occupied are compared. Based on the comparison, the map with maximum log-likelihood is taken as the temporary most likely map for the given sensor measurements.

The E and M steps can be explained using an example, where the the parameter values are shown in Table 4.1.

Table 4.1: Common simulation parameters for FSM-based occupancy map algorithm.

Parameter	Value	Parameter	Value
p_{rand}	0.5	Cell size, l	$1m$
p_{max}	0.3	Noise variance, σ^2	$1m$
p_{hit}	0.9	FoV	40 deg
z_{max}	$2.5m$	p_{ang}	0.86

Considering only one sensor measurement for the simplicity of calculations and the value of the measurement as $1.5m$. Considering that there are no other sensor measurements, it is expected that all cells falling on the sensor measurement arc are occupied. Now, the judgment of the E and M steps on the occupancy of cells falling on the measurement arc is explained below.

Let the map be initialized with no occupied cells. Therefore, the expectation for the non-random case is initially 0. That is,

$$e_{s,*} = 1,\ e_{s,0} = 0,\ e_{s,k} = 0.$$

Let the maximization function be denoted by J

$$\begin{aligned} J_0 &= e_{s,*} \log p(z_t|m, c_{s,*} = 1), \\ &= e_{s,*} \log \frac{1}{z_{max}}, \\ &= 1 \log \frac{1}{2.5 \times 10^2} = -5.5214. \end{aligned}$$

Since the measurement from the ultrasonic sensor is at centimeter level accuracy, the sensor range is taken in cm. Now, considering a temporary setting of occupancy state of the cell on the measurement arc to be occupied. The maximization can be calculated as

$$\begin{aligned} J_1 &= e_{s,*} \log p(z_s|m, c_{s,*} = 1) + e_{s,1} \log p(z_s|m, c_{s,1} = 1), \\ &= e_{s,*} \log \frac{1}{z_{max}} + e_{s,1} \log \frac{1}{\sqrt{2\pi\sigma^2}} e^{-\frac{(z_s - d_{s,1})}{\sigma^2}}. \end{aligned} \tag{4.36}$$

The expectations $e_{s,*}$ and $e_{s,1}$ can be calculated using (4.29) and (4.31).

$$\begin{aligned} e_{s,*} &= \eta \frac{1}{z_{max}} p_{rand}, \\ &= \eta \frac{0.5}{250} = \eta(2 \times 10^{-3}), \\ e_{s,1} &= \eta \frac{1}{\sqrt{2\pi\sigma^2}} e^{-\frac{\left(z_s - d_{s,1}\right)}{2\sigma^2}} (1 - p_{rand} - p_{max})(1 - p_{hit})^{s_k - 1} p_{hit} p_{ang}, \\ &= \eta(0.0686), \text{where } \eta = \frac{1}{0.0706}. \end{aligned}$$

Therefore, using $e_{s,*} = 0.0283$ and $e_{s,1} = 0.97167$ in (4.36),

$$\begin{aligned} J_1 &= 0.02832 \log \frac{1}{250} + 0.9716 \log \frac{1}{2\pi\sigma^2}, \\ &= -0.1758 - 0.89290 = -1.0687. \end{aligned}$$

Comparing the log-likelihood values for the no occupied cells and one occupied cell at measurement arc, $J_1 > J_0$. Therefore, the occupancy state of the considered cell remains occupied.

If another cell on measurement arc is checked for likelihood maximization, the occupancy state needs to be temporarily set to occupied and then the maximization function is calculated. If the cell is to termed as occupied, the function value for the cell being occupied should be greater than the function value obtained in the previous scenario ($J_2 > J_1$). The expectation values can be determined similar to the previous case. The stance for this cell is same as the stance number of the previous cell considered as both the cells are at same radial distance from the sensor position.

$$
\begin{aligned}
e_{s,*} &= \eta \frac{1}{z_{max}} p_{rand}, \\
&= \eta \frac{0.5}{250} = \eta(2 \times 10^{-3}), \\
e_{s,1} &= \eta \frac{1}{\sqrt{2\pi\sigma^2}} e^{-\frac{\left(z_s - d_{s,1}\right)}{2\sigma^2}} (1 - p_{rand} - p_{max})(1 - p_{hit})^{s_k - 1} p_{hit} p_{ang}, \\
&= \eta(0.0686), \\
e_{s,2} &= \eta \frac{1}{\sqrt{2\pi\sigma^2}} e^{-\frac{\left(z_s - d_{s,2}\right)}{2\sigma^2}} (1 - p_{rand} - p_{max})(1 - p_{hit})^{s_k - 1} p_{hit} p_{ang}, \\
&= \eta(0.0686), \text{where } \eta = \frac{1}{0.1392}.
\end{aligned}
$$

Therefore, using $e_{s,*} = 0.0144$, $e_{s,1} = 0.4928$ and $e_{s,2} = 0.4928$ in the maximization function,

$$
\begin{aligned}
J_2 &= e_{s,*} \log p(z_s|m, c_{s,*} = 1) + e_{s,1} \log p(z_s|m, c_{s,1} = 1) + e_{s,2} \log p(z_s|m, c_{s,2} = 1), \\
&= e_{s,*} \log \frac{1}{z_{max}} + e_{s,1} \log \frac{1}{\sqrt{2\pi\sigma^2}} e^{-\frac{(z_s - d_{s,1})}{\sigma^2}} + e_{s,2} \log \frac{1}{\sqrt{2\pi\sigma^2}} e^{-\frac{(z_t - d_{s,2})}{\sigma^2}}, \\
&= -0.9852.
\end{aligned} \tag{4.37}
$$

Clearly, $J_2 > J_1$; therefore, the occupancy of the second considered cell is also not flipped to empty as it maximized the likelihood function. Figures 4.5a shows the ground truth map with the obstacles shown in black and the markers representing the location of the sensor. The OG map generated is shown in Figure 4.5b. Since this mapping algorithm generates a binary map, the occupied cell are represented in black and the empty cells are white.

The above E and M-steps explained are iterated for all the cells, thereby generating various possible maps for the specified grid size. At the end of each iteration the temporary most likely map is found out. The whole algorithm ends when the map remains the same without any flipping of occupancy for any of the map cells. This is when the algorithm is termed to be converged. Once this convergence is reached, the algorithm produces the most likely map for the set of sensor measurements in a binarized representation of occupancy.

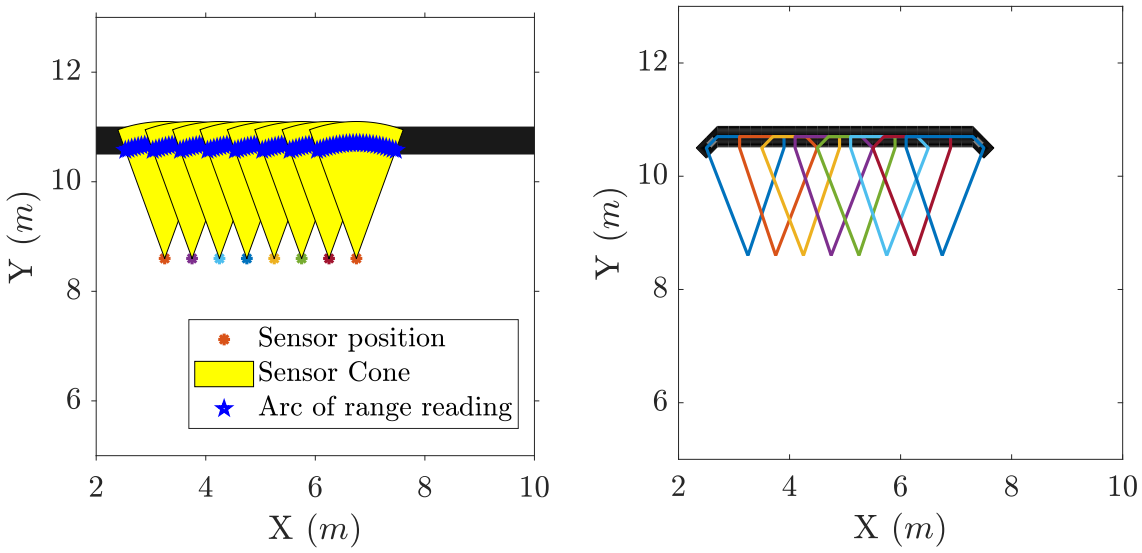

Figure 4.5: (a) Ground truth environment and sensor cones, (b) OG map generated using the FSM-based algorithm.

4.3 Conclusion

The inverse sensor model and the recursive update equation are formulated based on certain assumptions. These assumptions include neglecting dependence of neighboring cells' occupancy, not accounting for random measurements and other measurement aberrations. Owing to these assumptions, the ISM based mapping method is computationally inexpensive. However, on the downside, since the important characteristics of the sensor measurements are not considered, the occupancy certainty of the cells is questionable.

In contrast to the ISM, the FSM tracks the causes of the sensor measurement instead of interpreting the sensor information. In addition to this, the FSM based mapping considers most of the characteristics that are left over in the previous method. Necessary modifications to the basic FSM are incorporated in the description and corresponding probability distributions are derived for computing the expected log-likelihood. Furthermore, the EM algorithm is employed to solve the problem of maximizing the log-likelihood function with latent variables. Finally, for the ease of implementation, the framework of both the mapping algorithms are elaborated.

Algorithm 4.3: EM algorithm for occupancy mapping using multiple sensors

%% Initialization
for `all grid cells` **do**
  $m_{x,y} = 0$
end
repeat
  %% E-Step
  for `all measurements s from` 1 **to** N **do**
1 Calculate distances of obstacles in sensor cone;
    $e_{s,*} = \frac{1}{z_{max}} p_{rand}$
    $e_{s,0} = \frac{1}{\sqrt{2\pi\sigma^2}} e^{-\frac{(z_s - z_{max})}{2\sigma^2}} p_{max}$
    for `all k from` 1 **to** K_s **do**
      $e_{s,k} = (1 - p_{hit})^{s_k - 1} p_{hit} p_{ang} p\left(z_s | m, c_{s,k} = 1\right)$;
      If multiple obstacles are at same distance, then same priority is given (maintaining same value of k).
    end
    $\eta = \left[e_{s,*} + e_{s,0} + \sum_{k=1}^{K_s} e_{s,k}\right]^{-1}$;
    $e_{s,*} = \eta e_{s,*}$
    $e_{s,0} = \eta e_{s,0}$
    $e_{s,k} = \eta e_{s,k}$
  end
  %% M-Step
  repeat
    for `all grid cells <x,y>` **do**
      for `occupancy` $i = 0, 1$ **do**
2 $m_{x,y}^{[i]} = 0$;
        for `all measurements overlapping <x,y>` **do**
          Calculate D_s, K_s with $m_{x,y} = i$ in z_s;
          if $m_{x,y} = 0$ & $i = 1$ **then**
            recalculate $e_{s,k}$;
          end
          $m_{x,y}^{[i]} = m_{x,y}^{[i]} + e_{s,*} \log p(z_s | m, c_{s,*} = 1) + e_{s,0} \log p(z_s | m, c_{s,0} = 1)$
            $+ \sum_{k=1}^{K_s} e_{t,k} \log p(z_s | m, c_{s,k} = 1)$
        end
      end
      $\Delta_{x,y} = m_{x,y}^{[1]} - m_{x,y}^{[0]}$;
      if $\Delta_{x,y} \geq 0$ **then** $m_{x,y} = 1$;
      else $m_{x,y} = 0$;
    end
  until *convergence*;
until *convergence*;

Chapter 5

Performance Metrics for Generated Occupancy Maps

The previous chapter discussed the two different approaches of grid-based mapping; these are the inverse sensor model (ISM) and the forward sensor model (FSM) based OG mapping. While the FSM-based approach generates a binary map representing the surrounding environment, the ISM-based approach represents the map as probability values. To quantify the accuracy of the generated map, the maps need to compared to the ground truth map (GT). Thus, defining a set of metrics is necessary to compare the map generated from each method with the GT map. Analysis of these metrics aids in identifying the better of the two methods. Moreover, as the metric value quantifies the accuracy of the generated map, the influence of each algorithm parameters on the accuracy can be studied.

A metric defined for the above applications should possess the following basic properties:

- The metric accounts for the occupied cells which are out of reach for the vehicle sensors.
- The metric compares the exact position of the occupied cells.
- The metric measures the correctness and faults of the generated maps.
- The metric allows for the comparison of various methods to generate OG maps.
- The metric is able to quantify various characteristics of an OG mapping algorithm. Ability to judge correctly occupied cells, total error are a few characteristics of an OG algorithm.

In this chapter, before discussing the bench-marking suite for evaluating occupancy maps, the simulation setup and a test scenario for comparing OG maps are described.

5.1 Simulation Setup

To obtain a map of the environment, the ego vehicle must move through the free space and perceive its surroundings using the ultrasonic sensors. The ego vehicle is given a reference point in world coordinate system. Figure 5.1 shows the ego vehicle with one fixed sensor at two different positions in

the world co-ordinate system. Since the vehicle moves in x-direction, its velocity is contributed only by the x component. This velocity is written as

$$v_e = \frac{x_{v2} - x_{v1}}{t}, \tag{5.1}$$

where x_{v2} and x_{v1} are the positions and t is the time interval.

Considering only one sensor on the vehicle, the sensor also moves at the same speed of the vehicle. Now, let the sensor at two different positions detects an obstacle O. Let the actual obstacle co-ordinates be (x_o, y_o) with respect to the world frame. However, the sensor finds the distance of the obstacle relative to its position. Based on the measurement from the sensor, the obstacle coordinates can be determined. For the first measurement, let the obstacle co-ordinates determined using the measurement be (x_{o1}, y_{o1}). Similarly, for the second measurement, the obstacle co-ordinates are (x_{o2}, y_{o2}). Now, we can calculate the velocity of the obstacle given that we have the co-ordinates of the obstacle at two time instances. Therefore, the velocity of the obstacle in x and y direction is written as

$$\dot{x}_o = \frac{x_{o2} - x_{o1}}{t}, \tag{5.2}$$

$$\dot{y}_o = \frac{y_{o2} - y_{o1}}{t}. \tag{5.3}$$

Due to the assumption of static environment, the obstacle velocities are zero. Therefore,

$$x_{o2} = x_{o1} = x_o, \tag{5.4}$$

$$y_{o2} = y_{o1} = y_o. \tag{5.5}$$

Hence, the dependence of time interval is eliminated. To this end, instead of considering velocity as a function of time, the distance traveled alone is considered. From (5.1), considering the distance traveled,

$$d_i = x_{v2} - x_{v1}, \tag{5.6}$$

Here, d_i is termed as the inter-exploration distance. In the following chapters, the time dependence is eliminated and this inter-exploration distance is considered for exploring the surrounding environment.

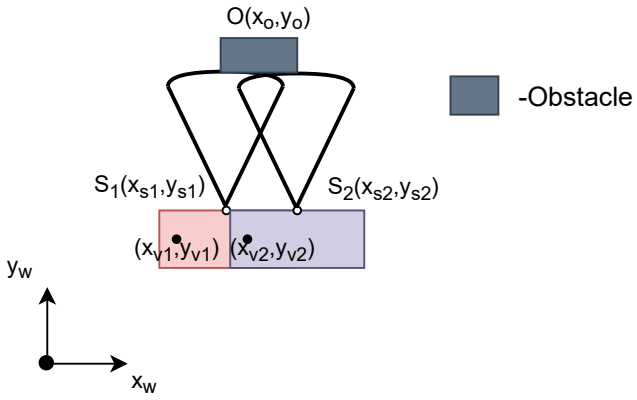

Figure 5.1: Sensor measurement in world co-ordinates.

5.2 Test Scenario for Evaluation OG Maps

Test scenarios test the potential of an occupancy mapping algorithm, and the metrics provide the measure of this potential. One of the important applications of an ultrasonic sensor is to aid the ego car in parking. Therefore, the test scenario is selected in such a way that it represents everyday parking events.

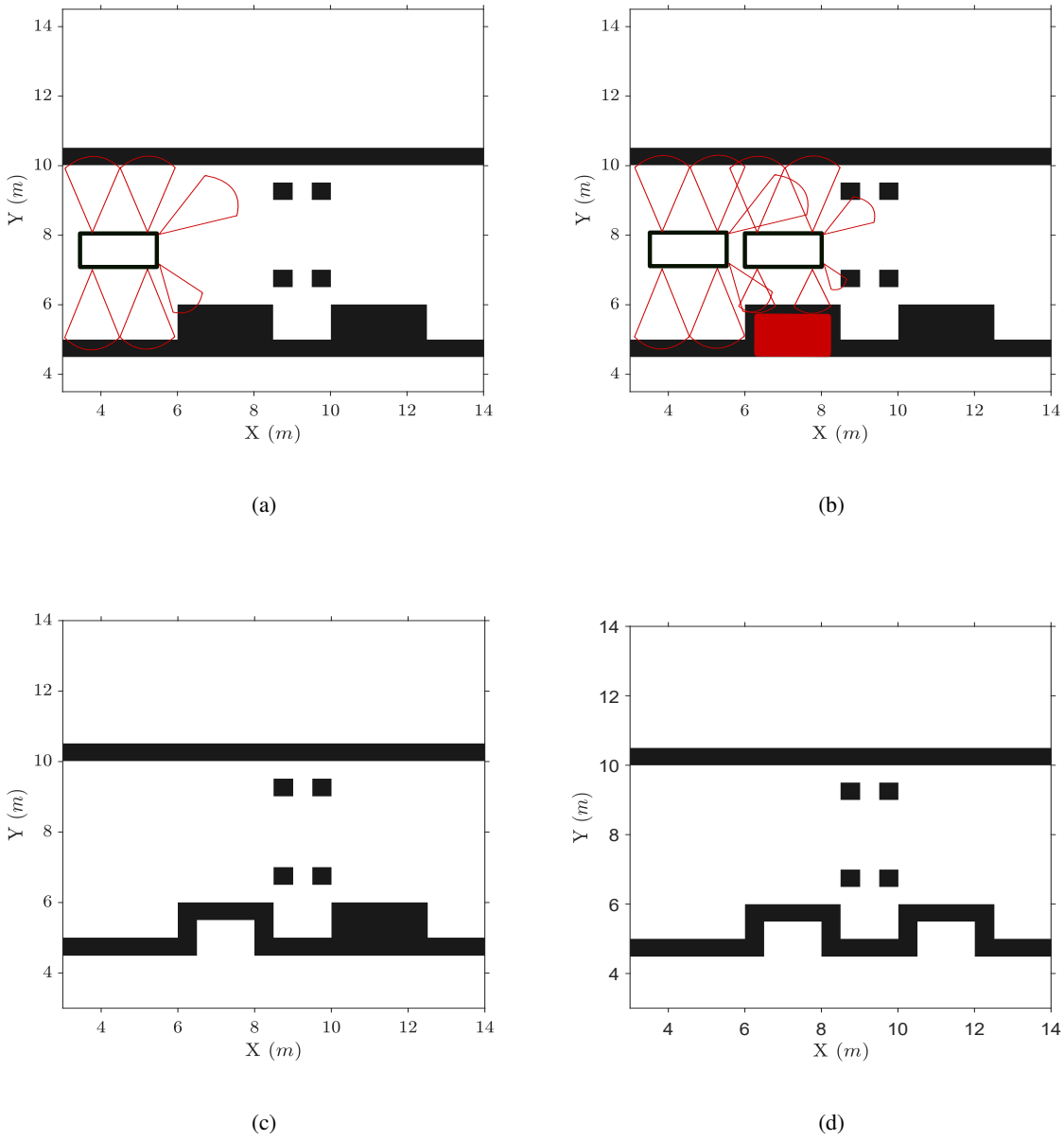

Figure 5.2: (a) GT map for a test environment, (b) area in red shows the unobserved area during exploration, (c) the unobserved area is removed, (d) the best observable GT map for the same test environment.

Figure 5.2a shows a test environment created to evaluate maps generated from the two algorithms presented in Chapter 4. This test environment poses a few challenges for mapping. These challenges include identifying small cluttered obstacles and obstacles behind these small cluttered obstacles. Six ultrasonic sensors are fixed around the vehicle for perception of the surrounding environment as shown in the figure. Although the actual physical environment could be similar to Figure 5.2a, the ego vehicle at its best could only see the physical environment as in Figure 5.2b. The area in red cannot be seen by the sensors from the explorable area. Hence, this area is not relevant while comparing the map generated for the available sensor measurements and the GT map. Therefore, Figure 5.2c shows the map after removing the red patch from the ideal GT map. A similar process is carried out throughout the map to obtain the best possible environment that can be perceived by the sensors. This best possible physical environment perceived by the ego vehicle is the observable map for the ideal GT map and is shown in Figure 5.2d.

5.3 Bench-marking Suite

In this section, various metrics are chosen from literature and modified to measure the quality of an occupancy map. These metrics are explained in detail in this section along with their applicability and features.

1. **Map Score (MS)** —The MS [26] is calculated by comparing two maps representing the same world. To compare two OG maps A and B for all cells i at a given instance, the MS denoted by κ_{MS} is calculated using

$$\kappa_{MS} = \sum_{i} \left[\log_2 \left(1 + A_i B_i + \bar{A}_i \bar{B}_i\right)\right], \tag{5.7}$$

   where $\bar{A} = 1 - A$ and $\bar{B} = 1 - B$.

   The MS is calculated for the occupancy maps represented in probability values, i.e, 0 to 1. These probability values can be very small numbers closer to 0; hence, mathematical operations on these probability values can lead to truncation error and higher computation complexity. For tackling these errors, a logarithmic approach is chosen.

   For the comparison of the generated map with the GT, only the cells of the GT that are observable by the sensors are considered. Therefore, the best observable map is constructed from the ideal GT, which takes only the observable cells into account. Furthermore, for comparing various generated OG maps having a different total number of cells, the MS is normalized. The normalized MS is written as,

$$\widehat{\kappa^t_{MS}} = \frac{\kappa^t_{MS}}{N_{tot}}, \tag{5.8}$$

   where N_{tot} denotes the total number of grid cells in the map considered.

   The MS metric yields the range of values between 0 and 1, when a probabilistic map is compared to GT map represented in binary form. Furthermore, if the two maps compared are exactly the same, then the MS is 1. On the other hand, if the maps compared are completely different, then the MS becomes 0. This implies that the higher the MS, the greater the similarity between the compared maps.

2. **Map Error (ME)** —Similar to the MS, the ME metric compares the two maps on a cell by cell basis. For each cell of the generated map, the difference in occupancy probability is calculated with respect to the observable GT map. The ME is the sum of all these differences.

   The mathematical representation of the metric calculated for all cells i of two maps A and B at any given instance is

   $$\Delta_{ME} = \sum_i |\,(A_i - B_i)\,|. \tag{5.9}$$

   Similar to the MS, for comparing multiple generated maps, normalization of the ME is necessary. This normalized ME is represented as

   $$\widehat{\Delta}^t_{ME} = \frac{\Delta^t_{ME}}{N_{tot}}, \tag{5.10}$$

   where N_{tot} is the total number of cells compared.

   If a binarized ground truth map is used for bench-marking, then the normalized ME could take values between 0 and 1. The map error value 0 implies that the generated map is exactly the same as the ground truth map, whereas a ME of 1 indicates that the generated map is completely contrasting to the GT map. Furthermore, if both the GT and the generated map are represented in binary form, then the total ME will be equal to the ratio of the number of cells falsely judged by the generated occupancy map to the total number of cells compared. Therefore, a lower ME indicates a better match of the generated map with the GT map.

3. **Kullback-Leibler (KL) Divergence** [27] —In general, the KL-divergence value is used to compare two probability distributions and provide a measure of how one probability distribution is different from the other. In case of comparison of an occupancy map, the generated map and the GT map represented in terms of probabilities need to be compared. The divergence metric calculated for all cells i of maps A and B at any given instance

   $$D_{KL}(A||B) = \sum_i A_i \log \frac{A_i}{B_i} + (1 - A_i) \log \frac{\bar{A}_i}{\bar{B}_i}, \tag{5.11}$$

   where $\bar{A} = 1 - A$ and $\bar{B} = 1 - B$.

   The parameter $D_{KL}(A||B)$ indicates that the metric value calculated is a divergence measure of the generated map B with respect to the benchmark map A. However, this divergence measure is not symmetric, i.e., the divergence from A to B is not the same as the divergence from B to A. Therefore, A denotes the GT map and B denotes the map generated from an OG mapping algorithm.

   In addition to the non-symmetric characteristic, one of the unique characteristics of this quantifier compared to the others discussed above is its ability to account for the over/under-estimation of occupancy by the generated occupancy map with respect to the GT map. The divergence value increases as a penalty depending on the difference between the probability values of the generated and the GT map cell. Therefore, an extremely high divergence value is an indication of a highly contrasting generated occupancy map with respect to the GT map.

   Similar to the previous metrics, in order to neglect the cells which are not explorable by the ego vehicle, the best observable map can be used instead of the ideal GT map for comparison. However, for comparing multiple maps with different number of cells, the normalization constant

used in previous metrics is not applicable for this quantifier. Therefore, this metric is only useful to compare maps of same size, dimensions and number of cells. Furthermore, there could be singularities while calculating the divergence value when the compared maps are represented in binary form. Therefore, to avoid singularities, the binary representation of the map using 0s and 1s are modified. A positive value very close to zero, which is almost insignificant, is added to the zeros (i.e., $0+\epsilon$) and the same ϵ value is subtracted from the ones (i.e., $1-\epsilon$). Despite the inapplicability of the metric to compare OG maps of different sizes, they are useful to compare probability OG maps with the same resolution.

One of the common tools used in describing the performance of a classification model is the confusion matrix [40]. For simplicity, a binary classification is chosen for comparing the maps. Therefore, the remaining metrics can be computed from a confusion matrix of size 2×2 for binarized GT and generated maps. Before discussing the list of metrics dependent on the confusion matrix, the confusion matrix needs to be constructed. For constructing the confusion matrix, the occupied cells are treated as the positive class and the empty cells are treated as the negative class. The GT map's classes are represented in each column of the matrix, while the generated map classes are represented in each row of the confusion matrix.

Table 5.1: Confusion matrix for comparing binarized occupancy maps.

		Ground Truth Map	
		Positive	Negative
Generated Map	Positive	True Positive (TP)	False Positive (FP)
	Negative	False Negative (FN)	True Negative (TN)

Table 5.1 shows the confusion matrix used to compute the remaining metrics. According to the confusion matrix, there are four possible outcomes when a cell from the generated map is compared with the GT map. These are

- *True Positive (TP)* —TP is an outcome when a cell from the generated map is correctly classified as occupied (positive).
- *True Negative (TN)* —TN is the case for a cell correctly classified as not occupied (negative).
- *False Positive (FP)* —If a cell is judged occupied (positive) in the generated map, but the same cell is not occupied in the GT map.
- *False Negative (FN)* —If a cell is judged empty (negative) in the generated map, but the same cell is occupied in the GT map.

Since the metrics derived from the confusion matrix are valid only for binary maps, the ISM generated map needs to be binarized. This binarization is carried out by choosing a threshold value. For example,

a cell with a probability of being occupied higher than 0.5 can be declared as occupied and otherwise it is declared empty. Furthermore, similar to other metrics, the best observable GT map can be used instead of the ideal GT map.

4. **Overall Error (OE)** [39] —The OE is the proportion of all incorrectly judged cells in the generated map compared to the GT map with respect to the total number of cells compared. The overall error (OE) at any given instance denoted by κ_{OE} is written as,

$$\kappa_{OE} = \frac{C_{FP} + C_{FN}}{N_{tot}}, \tag{5.12}$$

where N_{tot} denotes the total number of cells compared. Additionally, the term C is the number of cells in a class and the subscript of C denotes the class from the confusion matrix. For a generated map already in binary form, the OE is same as the normalized ME.

5. **True Positive Rate (TPR)** [39] —TPR is the ratio of TP classified cells to the total occupied cells in the GT map. This can be written as,

$$\kappa_{TPR} = \frac{C_{TP}}{C_{TP} + C_{FN}}. \tag{5.13}$$

κ_{TPR} quantifies the sensitivity of a mapping algorithm to correctly judge the occupied cells at a given instance . The number of cells belonging to the true positive class is represented by C_{TP}.

6. **False Positive Rate (FPR)** [39] —FPR is the ratio of FP classified cells to the total empty cells in the GT map. This measure is calculated as

$$\kappa_{FPR} = \frac{C_{FP}}{C_{FP} + C_{TN}}. \tag{5.14}$$

κ_{FPR} quantifies how often the generated map incorrectly classifies an empty cell as being occupied at a given instance. Understanding this quantifier also helps to understand the contributions to the OE from the class of FP and the FN implicitly.

5.4 Conclusion

To quantify the performance of a generated occupancy map with respect to the GT map, a set of metrics has been defined. The metrics are defined in such a way that each of the metric is able to quantify at least one of the key characteristics of the generated occupancy map. MS and ME metrics compares the generated map to the GT map on an overall level. The KL-divergence is a useful metric to compare maps with same resolutions. The divergence metric provides a measure on how bad the generated map estimates the occupancy states of the cells with respect to the benchmark map. This metric is useful particularly for probability-based maps as the divergence value increases as a penalty depending on the difference between the probability values of the generated and the GT map cell.

Three other performance metrics are defined based on the confusion matrix constructed for comparing two binarized occupancy maps. The three metrics quantifies the overall error, sensitivity of an algorithm to judge occupied cells and the rate at which an algorithm wrongly judges an empty space

as occupied. The three metrics provide evidence for the trends in overall performance metrics. Furthermore, an example of a challenging scenario including its observable representation to evaluate the generated occupancy maps is also presented. The metrics defined in this chapter along with the test scenario is useful to analyze the performance of the occupancy maps generated from different mapping algorithms.

Chapter 6

Performance Evaluation of the Mapping Algorithms

For comparing the generated occupancy maps with the ground truth (GT), a set of metrics is presented in Chapter 5. Based on the defined metrics, the performance of the occupancy grid (OG) mapping algorithms are studied in this chapter. The performance of a mapping algorithm is influenced by the parameters in the algorithm. In Section 6.1, the parameters potentially influencing the performance of the inverse sensor model (ISM) and the forward sensor model (FSM) based mapping methods are identified. In Section 6.2, the consistency of the explorable area for the observable GT maps is validated for a test scenario. The influence of the identified parameters on the performance of the ISM and the FSM based algorithms are discussed in Sections 6.3 and 6.4, respectively. Finally, the two methods for occupancy mapping are compared using the performance metrics for a given test scenario in Section 6.5.

6.1 Parameters Influencing Performance of the Mapping Algorithms

Based on the ISM and its occupancy mapping algorithm discussed in Chapter 4, the parameters potentially influencing the performance of this algorithm are listed in Table 6.1. The table categorizes the parameters based on their relation to the algorithm components. Field of view (FoV), sensor range and the probability parameters (p_{emp}, p_{occ}) are all related to the characteristics of the ultrasonic sensor. The values of FoV and the sensor range are explicitly available in the specification sheet of the sensor [7], whereas the probability values can be well determined through an empirical approach [39]. Due to unavailability of the hardware in this graduation project, these probability values are adopted from the literature [27]. Therefore, the remaining parameters which can affect the performance of the algorithm are the grid resolution of the generated occupancy map and the inter-exploration distance. These two parameters are considered for further analysis.

Similar to the ISM, the list of parameters potentially influencing the performance of the FSM based algorithm is presented in Table 6.1. Here, in addition to the common sensor parameters such as the FoV and the sensor range, the algorithm specific parameters are also listed under the sensor category. These parameters are noise variance, probability of the sensor yielding a random (p_{rand}) and a max-range (p_{max}) measurements. Furthermore, if the sensor produces a non-random measurement,

then the probability that it detects the closest occupied cell is p_{hit}. All these parameters can also be determined from experiments. However, similar to ISM, these parameters are adopted from the literature [39]. The remaining parameters are the same as in the ISM and are discussed in detail in the forthcoming paragraphs.

Table 6.1: Parameters potentially influencing the performance of ISM and FSM-based algorithms.

Category	Parameters in ISM-based algorithm	Parameters in FSM-based algorithm
Sensor	Field of view (FoV) Sensor range p_{emp} p_{occ}	Field of view (FoV) Sensor range Noise variance (σ^2) p_{rand} p_{max} p_{hit}
Map	Grid resolution	Grid resolution
Vehicle	Inter-exploration distance	Inter-exploration distance

The first parameter potentially influencing the performance of a mapping algorithm is the grid resolution. Occupancy grid maps represent the environment in the form of uniform shaped cells with same size [28]. The resolution of these maps is decided by fixing the cell size, which is denoted by l. An occupancy map can be of high/low resolution compared to another based on the comparison of the cell sizes. Consider two occupancy maps of equal total area A and B where the map A is said to have a higher resolution than map B if the cell size of A is smaller than the cell size of B and vice-versa. A right value of the cell size is important for efficient occupancy mapping. For instance, in a low-resolution map, since only one occupancy probability is stored and updated per cell, a partially occupied cell can be interpreted as completely occupied or empty (as shown in Figure 6.1a). This can lead to inconsistencies in the map. Whereas, in a high resolution map, unnecessary computation is spent on all the small cells if a large obstacle is present over many cells, as represented in Figure 6.1b. In addition to the computation involved, the performance of the mapping method can also be affected by the grid size. For small grid size, the cells falling on a measurement cone contributes to very accurate area covered by the sensor cone. On the other hand, the area covered by the sensor cone changes as the grid size increases. Furthermore, probability of the cells covered in the area is determined by the mapping methods and the sensor measurements. Therefore, the computation involved, performance of a mapping method all depend on the grid resolution.

Another parameter that can influence the performance of a mapping algorithm is the inter-exploration distance, which is the distance between two consecutive positions of the vehicle while exploring the surrounding environment. In other words, the inter-exploration distance is the distance traveled by the vehicle during the fixed sample time of the sensor. The distance traveled during this time depends on the velocity of the vehicle. In this research, in order to eliminate the dependency of time while exploring the environment, the sensor measurements are obtained at each new position of vehicle as a function of the inter-exploration distance. Therefore, the distance parameter affects the total number of sensor measurements obtained within a fixed length of exploration. A basic formula to compute the number of sensor measurements for a given start and end points of exploration for a fixed inter-exploration distance is written as,

$$S_{tot} = \left(\left\lfloor \frac{E_{end} - E_{start}}{d_i} \right\rfloor + 1 \right) S_v. \tag{6.1}$$

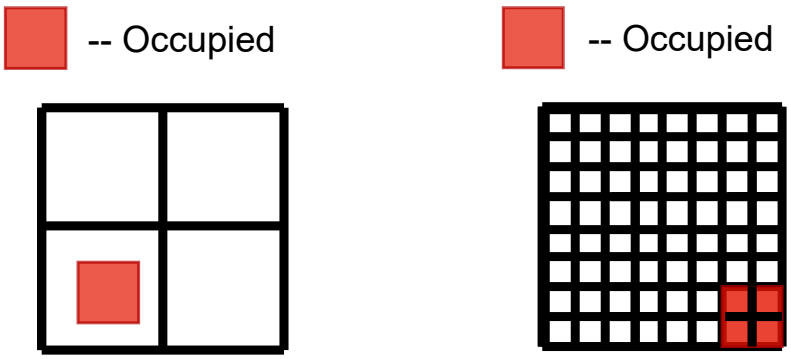

(a) (b)

Figure 6.1: A small area with various possible grid resolutions: (a) an obstacle partially occupied in a large grid cell, (b) an obstacle covering four grid cells owing to very high resolution.

Here, S_{tot} is the total number of sensor measurements picked up during the exploration of the environment by the vehicle. S_v is the number of sensors equipped in the vehicle. E_{start} and E_{end} are the start and end points of the exploration, which is used to determine the length of the exploration path. The parameter d_i denotes the inter-exploration distance. For instance, if a vehicle with six sensors explores a long passage from $1m$ to $10m$ with a fixed inter-exploration distance of $1m$, then there will be 60 sensor measurements in total at the end of the exploration.

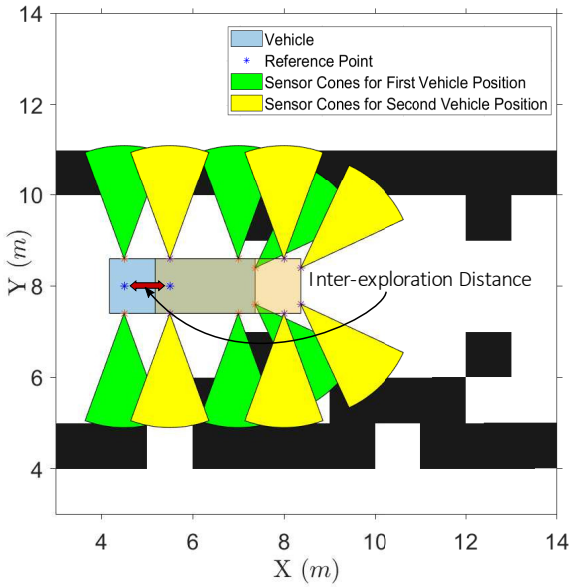

Figure 6.2: Simulation environment with a vehicle fixed with six ultrasonic sensors. The inter-exploration distance is marked for two consecutive exploration points.

Although a large number of sensor measurements aids in obtaining the most accurate map, it could lead to excessive computations. Therefore, finding the number of sensor measurements sufficient to provide an accurate map could reduce the exploration time and the computation.

Figure 6.2 shows a vehicle with six fixed sensors placed in a simulation environment. In this simulation, the vehicle explores in a straight line, where the inter-exploration distance affects only the x position of the vehicle. To carry out the exploration with a fixed inter-exploration distance, a reference point for the vehicle and the sensor is introduced. The blue marker in the figure is the reference point for the vehicle and the sensors during the simulations. The reference point is shifted to a distance equal to the defined inter-exploration distance. Relative to the reference point the vehicle and the equipped sensors are also shifted to explore the environment.

6.2 Test Maps - GT and Observable GT Maps

To analyze the performance of a mapping algorithm, the map generated using the algorithm should be compared with the benchmark map. The metrics defined in Chapter 5 are used for this analysis. One of the important prerequisites of the metrics for comparing the generated map with the benchmark is to have exactly the same number of cells. Therefore, for different generated maps, the number of GT map cells changes according the grid resolutions. However, the features in the GT map should not change with the change in grid resolution.

Another prerequisite for comparison using the metrics is the requirement of the best observable GT map. The use of an observable GT is to account for the cells that are not perceivable by the sensors from the explorable area. The observable GT map changes according to the grid resolution of the generated map. This change is due to the procedure carried out, where only the first row of perceivable cells are retained and the other cells are made empty. Figure 6.3 shows the various observable GT maps for different resolutions.

To check the consistency of the explorable area present between the walls in all the observable GT maps, the occupancy states of the cells are inverted. Figure 6.4 shows the occupancy map after inverting the occupancy states of the cells in the explorable area and the occupied area. The explorable area can also be calculated to cross check the visual representation. The formula for calculating the explorable area is written as,

$$A_{Exp} = N_{emp} l^2, \tag{6.2}$$

where A_{Exp} is the explorable area calculated and N_{emp} denotes the total empty cells in the explorable area. The parameter l represents the dimension of the cell.

At the simulation level, for testing the mapping algorithms, the accurate map of the GT is available directly. However, in a practical scenario, the accurate map of the surroundings may not be available directly. Therefore, a special bench-mark map is required to compare the maps generated from different mapping algorithms. Generating this bench-mark map is considered out of scope for this project; however, this is certainly one of the important recommendations from this project.

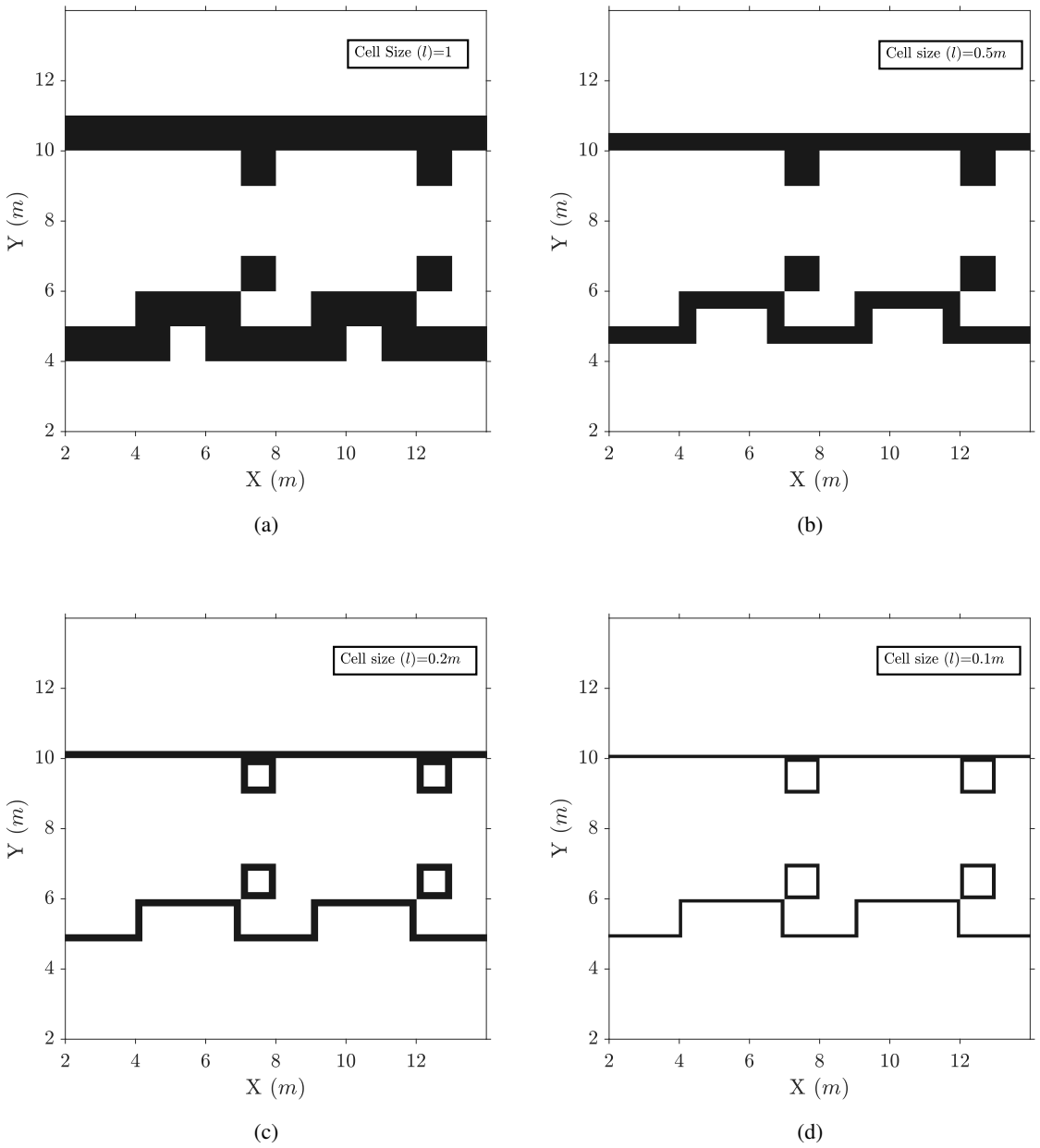

Figure 6.3: (a) GT map for a test environment with cell size (l) of $1m$, (b) observable GT map with $l = 0.5m$, (c) observable GT map with with $l = 0.2m$, (d) observable GT map with with $l = 0.1m$.

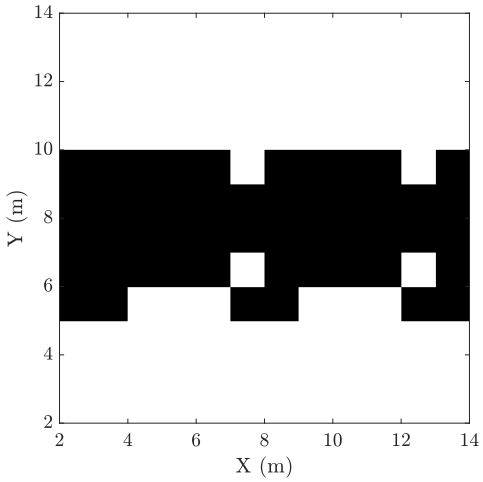

Figure 6.4: Inverted occupancy states for the explorable area and the occupied area.

6.3 Influence of the Parameters on the Performance of ISM Method

To investigate the influence of the grid resolution, various cell sizes are chosen and the corresponding occupancy maps are generated. The set of cell sizes chosen for this investigation is $\{0.1m, 0.2m, 0.5m, 1m\}$. All other parameters, including the inter-exploration distance, are kept constant during the investigation. Table 6.2 shows the common simulation parameters for generating ISM based maps. Furthermore, $1m$ inter-exploration distance is maintained while investigating the performance of the mapping method for different cell sizes. In fact, the inter-exploration distance value does not affect the trend in which the grid resolution influences the performance of the ISM based method, as shown in Appendix C.

Table 6.2: Common simulation parameters for ISM-based occupancy map algorithm.

Parameter	**Value**	**Parameter**	**Value**
Map width	$12m$	Vehicle start position	$4m$
Map length	$12m$	Vehicle end position	$9m$
Map origin	$[2, 2]$	Field of view (FoV)	$40deg$
Sensor range	$2.5m$	Initialization for all grid cells, $m^0_{x,y}$	0.5

Similar to the grid resolution, the influence of the inter-exploration distance on the performance of the ISM based method is examined by varying this parameter and analyzing the metrics for the corresponding generated occupancy maps. The set of inter-exploration distances chosen for this analysis is $\{0.1m, 0.25m, 0.5m, 1m, 1.5m, 2m, 2.5m, 3m\}$. During the analysis, the parameter values shown in Table 6.2 are used. The cell size for the simulation is also kept constant; however, the value is chosen based on the conclusion from the analysis of grid resolution. In this case as well, the trend in which the inter-exploration distance influences the performance is not affected by the value of the cell size chosen.

The cells of the occupancy map to be generated are initialized with a probability of 0.5 for the ISM-based mapping method. This implies that the occupancy states of all the cells are uncertain at the start of exploration. If the probability value of a cell does not change after the exploration and mapping processes, then it can be that the cell is either unexplored or there is no clear evidence to modify the occupancy state of the cell. The evidence here refers to the sensor measurements obtained during the exploration.

For the metrics based on the confusion matrix in Table 5.1, the ISM generated map should be binarized. For binarizing the generated occupancy map, a threshold of 0.5 is chosen. As a result, the binarization for all cells indexed (x, y) of the generated map is written as,

$$m_{x,y} = \begin{cases} 0, \text{if } m_{x,y} \leq 0.5, \\ 1, \text{if } m_{x,y} > 0.5. \end{cases} \tag{6.3}$$

The metrics determined using the confusing matrix do not provide information of the actually occupied area that are judged as uncertain by the mapping algorithm. To obtain this information, instead of the binarization process performed previously, a MAP decision rule is used. The decision rule is

$$m_{x,y} = \begin{cases} 0, \text{if } m_{x,y} < \bar{m}_{x,y}, \\ 1, \text{if } m_{x,y} > \bar{m}_{x,y}, \\ 0.5, \text{if } m_{x,y} = \bar{m}_{x,y}, \end{cases} \tag{6.4}$$

where $m_{x,y}$ is the probability of the cell (x, y) and $\bar{m}_{x,y} = 1 - m_{x,y}$. The map generated after applying the above decision rule is now compared with the GT map. The total number of cells that are occupied in the GT map but judged uncertain in the generated map is determined. Hence to account for these cells, a new metric in addition to the metrics defined in Section 5.3 is introduced. The metric to account for the uncertain cells is the uncertainty rate (κ_{UR}) and for any given instance it is written as,

$$\kappa_{UR} = \frac{C_u}{P}. \tag{6.5}$$

C_u is the total number of uncertain cells in the generated map that are actually occupied with respect to the GT and P is the total occupied cells in the GT map. This metric is used only for the special case of analyzing non-binarized maps that are initialized with a probability value of 0.5.

6.3.1 Grid Resolution

The influence of the grid resolution on the performance of the ISM based method is examined with the help of the metrics determined for the generated maps. All the metric values except for the Kullback-Leibler (KL) divergence are determined for the generated occupancy grid maps for the test scenario shown in Figure 6.3 considering various cell sizes. The KL divergence metric is not considered for this analysis as it does not account for the number of map cells for comparing various maps, i.e., not normalized. The various metrics obtained for the maps generated at the end of the exploration are represented in Figure 6.5. While Figure 6.5a represents all the metrics that are directly dependent on the performance, Figure 6.5b represents the metrics having inverse dependence on the performance. For in depth analysis of the ISM based method, the metrics are determined at each update of the occupancy map and are presented in Appendix B.

The normalized map score (MS) and the normalized map error (ME) are shown in Figures 6.5a and 6.5b, respectively. The metric lines corresponding to MS and ME are almost straight. This implies that there is no drastic influence of the cell size on the overall performance for the chosen values. This could be caused by dominance of number of empty cells in the GT map compared to the number of occupied cells. The remaining metrics need to be analyzed for understanding the characteristics of the method and its ability to judge occupancy of spaces.

The uncertainty rates (UR) obtained for various generated maps are plotted in Figure 6.5b. It can be seen that the UR decreases as the cell size increases. The higher the UR, the higher the uncertain cells that are actually occupied. This implies that at low values of cell sizes, a lot of occupied space can be left unexplored. Usually, for a high grid resolution, the area covered by the sensor cone is less compared to the area covered for low resolution; hence leading to higher values of UR for high resolutions. Furthermore, the effect of fine discretization of space is that even a very small unexplored region may result in the occupancy of many cells uncertain.

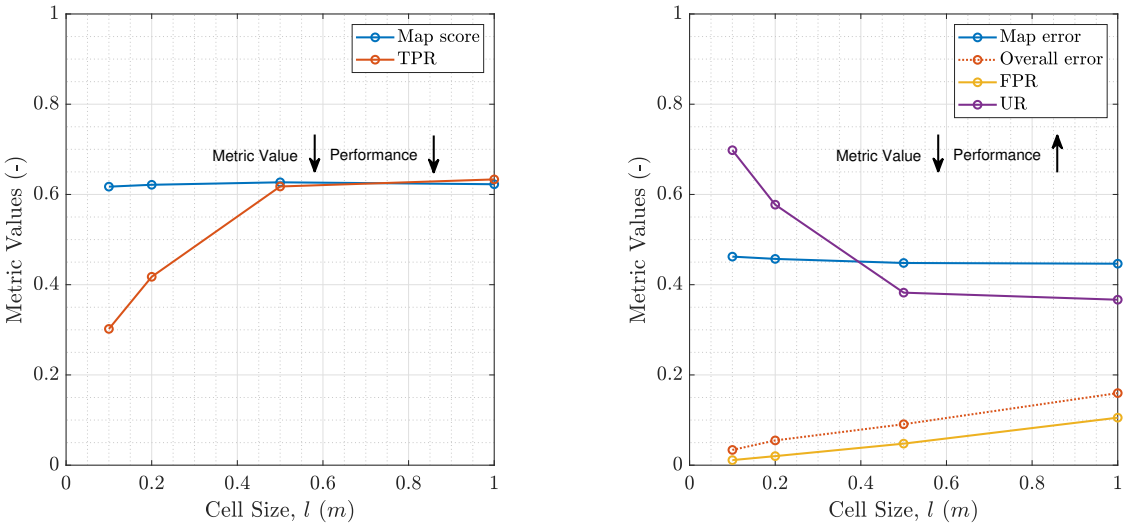

(a) (b)

Figure 6.5: Metric values for the occupancy maps with different cell sizes: (a) normalized MS and TPR and (b) normalized ME, OE, FPR and UR values for various occupancy maps generated for corresponding cell sizes.

The true positive rate (TPR) and the false positive rate (FPR) are plotted in Figure 6.5a and 6.5b, respectively. It can be seen that for small cell sizes, both the TPR and FPR are low. This implies that there is very little occupied space that is identified. The complementary of TPR is the false negative rate (FNR) and the complementary of FPR is the true negative rate (TNR). Low values for both the FPR and TPR implies high values of TNR and FNR. Therefore, a high value of FNR implies that most occupied cells are judged empty incorrectly. It is to be noted that even the unexplored/uncertain cells contribute to the empty cells in the binarized generated map. On the other hand, as the cell size increases, both the TPR and FPR increases. The increase in number of occupied cells is caused by increase in the area covered by the sensor cone. The increase in area is also evident from the decrease

in the UR.

The final metric is the overall error (OE), which is contributed by the false positive (FP) and false negative (FN) classified cells. It can be seen that the OE line increases with almost same trend as the FPR. For cell sizes 0.5 and $1m$, the TPR is almost constant. This implies that the FNR is also constant. Therefore, the main contribution to OE for cell sizes $0.5m$ and $1m$ is from FP cells.

To conclude, lower resolution maps have lower URs and better TPR (better performance) compared to the high resolution maps. In addition, considering the fact that TPR is almost same for $0.5m$ and $1m$ cell sized maps and the map generated for $0.5m$ cell size has lower FPR and OE (better performance), $0.5m$ cell size is the right value for the map generated from ISM based method.

6.3.2 Inter-exploration Distance

The inter-exploration distance affects the total number of sensor measurements obtained after the exploration. The total number of sensor measurements can be determined using (6.1) and the relevant simulation parameters values from Table 6.2. Furthermore, the cell size of $0.5m$ is kept constant for this analysis. For analyzing the influence of the distance parameter, the metric values are determined for the occupancy maps generated at the end of exploration. Figure 6.6 shows all the metric values, except for the KL-divergence, obtained for the occupancy maps. The metrics are grouped in such a way that Figure 6.6a is for the metrics having direct dependence on the performance, i.e., indicate better performance as the metric value increases. On the other hand, Figure 6.6a displays the metrics having inverse dependence on the performance.

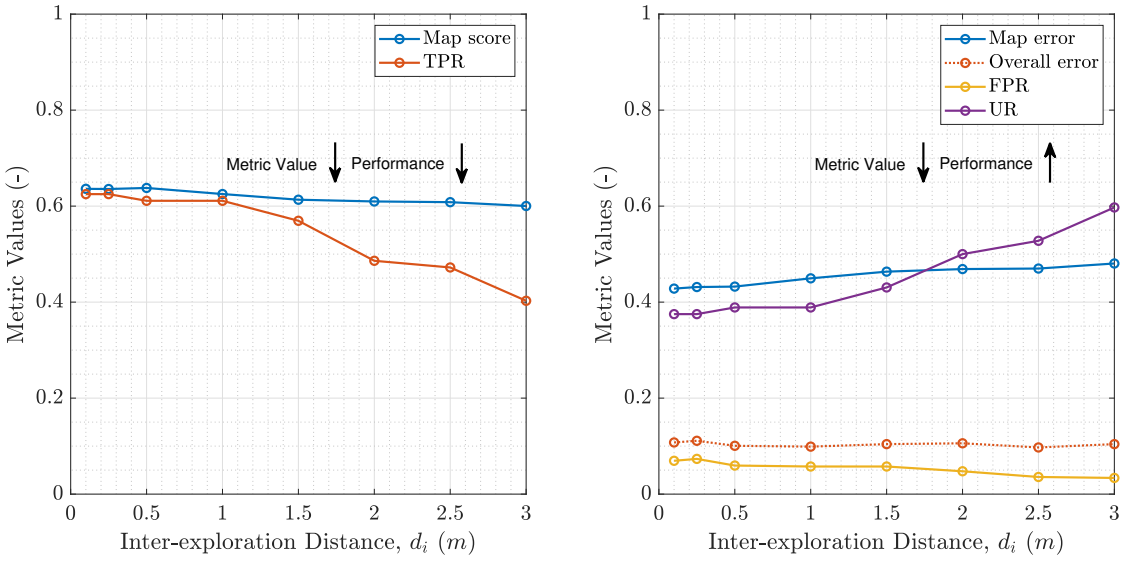

Figure 6.6: Metric values for the occupancy maps with different inter-exploration distances: (a) MS TPR and (b) ME, OE, UR and FPR values for various occupancy maps generated for corresponding inter-exploration distance.

Figures 6.6a and 6.6b show a slight decrease in the MS and a slight increase in the ME, respectively, with increasing inter-exploration distance. This characteristic is expected as the total number of sensor measurements decreases with increase in the distance. This also implies that the overlapping regions between the old and new measurements decreases, and in the worst case of large inter-exploration distance, there can be no overlapping regions. In addition to absence of overlapping, there will be unexplored regions in between the exploration steps. The increase of unexplored region with increase in inter-exploration distance is explained by the UR. The UR in Figure 6.6b shows an upward trend with increase in inter-exploration distance. Similar to MS and ME, the decrease in the performance with increase in the inter-exploration distance is also evident from the decreasing TPR in Figure 6.6a. This decrease in TPR is also a result of increase in the UR.

Although a few metrics discussed above indicated deteriorating performance with increase in the inter-exploration distance, an interesting behavior is observed for the KL-divergence line plot shown in Figure 6.7. The divergence value is high for small inter-exploration distance and settles for the inter-exploration distance of $1m$. After the critical distance of $1m$, the divergence line remains fairly straight. The initial surge in the divergence value is due to the highly confident (probability close to 0 or 1) false positive/false negative cells in the generated occupancy map. The higher the deviation between the generated and the GT map cell probabilities, the higher will be the divergence value. In addition to this, the more the number of highly confident false judged cells, the higher will be the divergence value.

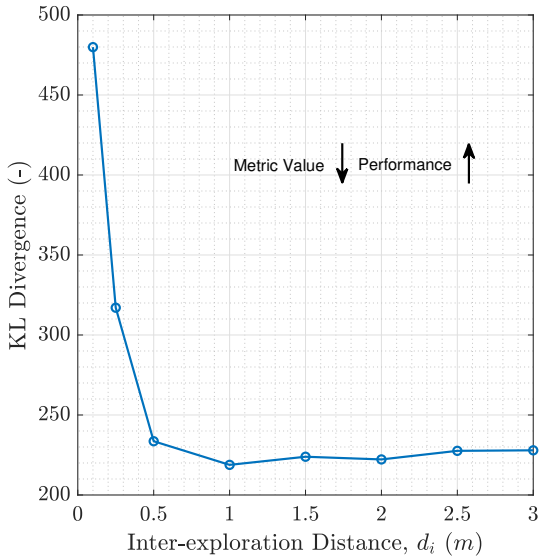

Figure 6.7: KL-Divergence values for generated map corresponding to various inter-exploration distances.

At $0.5m$ inter-exploration distance, the number of false positive cells decreases owing to decrease in the number of sensor measurements. However, a slight increase in UR is also seen at the same time. This increase implies that a little area can be unexplored compared to the occupancy map generated for inter-exploration distances of $0.25m$ and $0.1m$. At $1m$ inter-exploration distance, the KL-divergence settles to a lower value indicating that the number of highly confident false judged cells decreases with an increase in the uncertainty rate.

To conclude, despite the indication of good performance by MS and ME at very low inter-exploration distances, the KL-divergence shows that a lot of cells are incorrectly judged with high confidence. This incorrect judgment can be risky if a path needs to be planned based on the generated occupancy map. Therefore, it is better to have uncertain regions rather than incorrectly judged regions. In addition to this, if the inter-exploration distance is large, then the time to explore will also be less. Based on the analysis performed, the inter-exploration distance of $1m$ is appropriate. At this distance, neither the UR nor the KL divergence is high. Also, the metric values for the MS, ME and TPR show a good performance of the mapping algorithm

6.4 Influence of the Parameters on the Performance of FSM Method

As discussed in Section 6.1, besides the sensor related parameters, the other potentially influencing parameters are grid resolution and the inter-exploration distance even for the FSM-based occupancy mapping algorithm. Table 6.3 shows the common parameters and their values. These values do not change during the investigation of the parameters' influence on the performance of the algorithm. Furthermore, while investigating one of the parameters, the other parameters are kept constant.

The set of cell size values considered for investigating the influence of grid resolution on the performance is $\{0.1m, 0.2m, 0.5m, 1m\}$. During this investigation, the inter-exploration distance is maintained as $1m$. In fact, the value of inter-exploration distance is not of concern as the trend in which the grid resolution influences the performance is not affected by the value chosen. This is also explained in Appendix C. On the other hand, for investigating the influence of inter-exploration distance, the set of values chosen is $\{0.1m, 0.25m, 0.5m, 1m, 1.5m, 2m, 2.5, 3m\}$.

Table 6.3: Common simulation parameters for FSM-based occupancy map algorithm.

Parameter	Value	Parameter	Value
Map width	$10m$	p_{hit}	0.9
Map length	$10m$	p_{rand}	0.3
Map origin	$[2, 2]$	p_{max}	0.3
Sensor range	$2.5m$	Vehicle start position	$3m$
Noise variance (σ^2)	$1m$	Vehicle end position	$6m$
Field of view FoV	$40deg$	Initialization for all grid cells, $m_{x,y}$	0

6.4.1 Grid Resolution

For investigating the influence of grid resolution, the metrics defined in Chapter 5 are determined for the occupancy maps generated for the various cell sizes. Similar to the analysis of cell size on ISM based method, all the metrics except for KL divergence metric are determined. Figures 6.8 shows the results of evaluation of occupancy maps corresponding to the various choices of cell sizes. While Figure 6.8a consists of the results of the metrics that directly depend on the performance, Figure 6.8b shows the results of the metrics that have inverse dependence with the performance.

Figure 6.8a shows the results of the MS obtained for the various occupancy maps corresponding to the various choice of cell sizes. It can be seen that the MS has a decreasing trend as the grid resolution

of the generated occupancy map becomes low. This implies that the performance of the FSM-based method degrades with lower grid resolutions. In conformance with the behavior of the MS, the ME and OE also show an increasing trend (poor performance) in Figure 6.8b. This increasing trend of the ME and the OE means that the performance lowers as the grid resolution lowers. It can also be seen that the OE metric line overlaps the ME metric line. The reason for this overlap is the binary representation of the generated occupancy map. While the normalized ME is the ratio of total error to the total number of cells being compared, the OE is the ratio of total number of false classified cells to the total number of cells compared. However, due to binary representation of the generated occupancy map, only the false classified cells lead to an increase in the map error.

Figure 6.8a and 6.8b also show the TPR and the FPR, respectively. An increasing trend in the TPR can be seen until the occupancy map cell size is $0.5m$. Thereafter, for the cell size of $1m$, the TPR decreases. This implies that for the map with $1m$ sized cells, the mapping algorithm finds less number of correctly occupied cells. This is also evident from almost same range of FPRs for $0.5m$ and $1m$ cell sized maps. Furthermore, a distinct FPR and OE implies that there is a significant contribution from false negative cells in addition to the false positive cells. The OE metric line and the FPR diverges drastically for occupancy map of cell size $1m$. This divergence indicates that many of the empty cells in the generated occupancy map are also wrongly judged. Clearly, from the TPR and FPR values for the generated occupancy map of cell size $1m$, the judgment of empty and occupied cells are not correctly judged and have been mismatched to a great extent. This mismatch of occupied and empty cells also led to a lower performance of the mapping method.

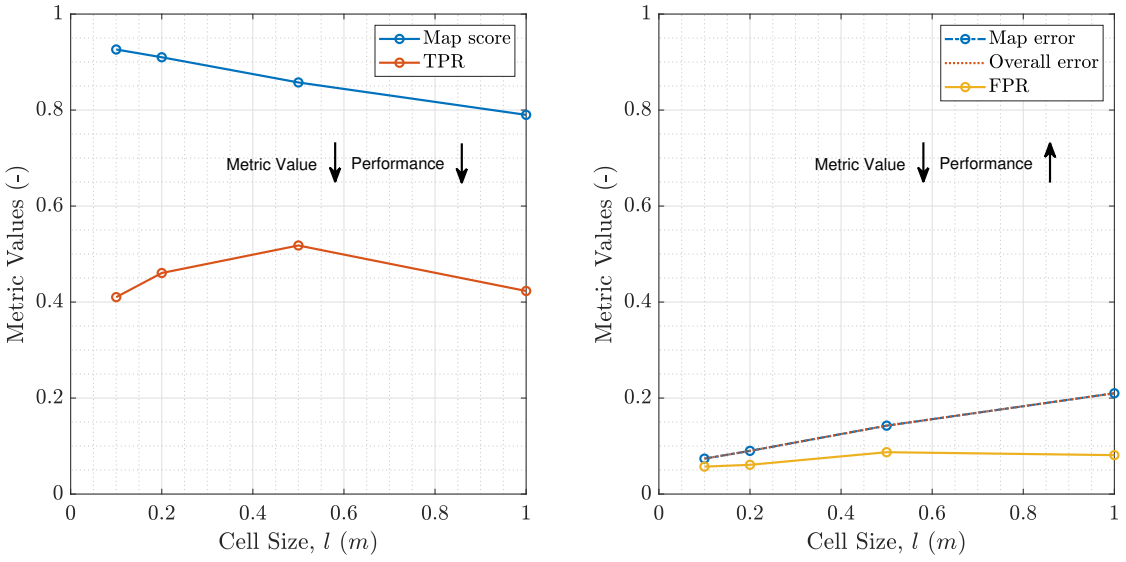

(a) (b)

Figure 6.8: Metric values for the set of cell sizes: (a) Normalized MS and TPR values, (b) Normalized ME, OE and FPR values for various occupancy maps generated for corresponding cell sizes.

One of the disadvantages of the FSM based mapping algorithm is the higher computation time. This algorithm iterates on all possible maps from the high-dimensional space for determining the map

that maximizes the likelihood of the obtained sensor measurements. The number of possible maps increases as the resolution increases. As a higher resolution map has more number of cells, the number of possible combinations of the cells being occupied increases. Therefore, the algorithm takes higher computation time for high resolution maps.

To conclude, despite better overall performance at high resolutions, the computation time increases as the cell size decreases for the same map size. On the other hand, the low resolution map of cell size $1m$ shows poor performance as there is clear mismatch of the occupied cells positions. Hence, as a trade-off between computation time and performance, the generated map with cell size $0.5m$ is the correct choice.

6.4.2 Inter-exploration Distance

For investigating the influence of the inter-exploration distance on the performance of the FSM-based algorithm, occupancy maps are generated for various values of the inter-exploration distance and the common simulation parameters in Table 6.3. In addition to the common simulation parameters, based on the analysis performed in the previous section, the cell size of $0.5m$ is fixed while investigating the influence of the inter-exploration distance. Figure 6.9 shows the obtained metric values for the generated occupancy maps corresponding to the chosen inter-exploration distances. The metric values having direct dependence on the performance are plotted together in Figure 6.9a. On the other hand, the metrics having inverse dependence on the performance are plotted together in Figure 6.9b.

The MS and the ME values are plotted in Figures 6.9a and 6.9b, respectively. The metric values do not change drastically for occupancy maps corresponding to various inter-exploration distances. Therefore, there is not much of influence of the inter-exploration distance on the overall performance. The observed negligible change in these metrics is due to lower occupied area compared to the empty area. Furthermore, all the occupancy maps generated judged most of the empty spaces correctly. This is supported by close metric lines corresponding to the OE and the FPR as they indicate a lower contribution of false negative cells to the OE. The OE and the ME overlaps in this case as well due to the binary nature of the generated occupancy maps.

Another interesting observation from Figure 6.9a is the fall in TPR for occupancy maps generated with inter-exploration distances more than $1.5m$. In addition to this behavior, the divergence of the OE and FPR lines increases for the maps with inter-exploration distances more than $1.5m$. This divergence indicates increase in FN cells. These behaviors are attributed to low area coverage and insufficient sensor measurements with the map being initialized as completely empty. Therefore, most of the cells remain empty as there are less or no measurements falling on the cells.

In addition to the metrics discussed above, the KL divergence metric is also determined for this analysis. Since both the FSM generated map and the GT map are in a binary representation, the occupancy values $0s$ and $1s$ are changed to 0.01 and 0.99 for determining the KL divergence. This change is required to eliminate the condition of singularities in the equation of the KL divergence metric. Figure 6.10 shows the KL divergence metric obtained for the occupancy maps. In the case of low inter-exploration distances (less than $1m$), the divergence values are high. The reason for this high divergence is the incorrect cells classified by the generated map. The divergence value reaches a low for the occupancy map generated with an inter-exploration distance of $1m$. This indicates that this occupancy map matches the GT map better than any other generated occupancy maps. The high divergence values for large inter-exploration distances is due to less explored areas.

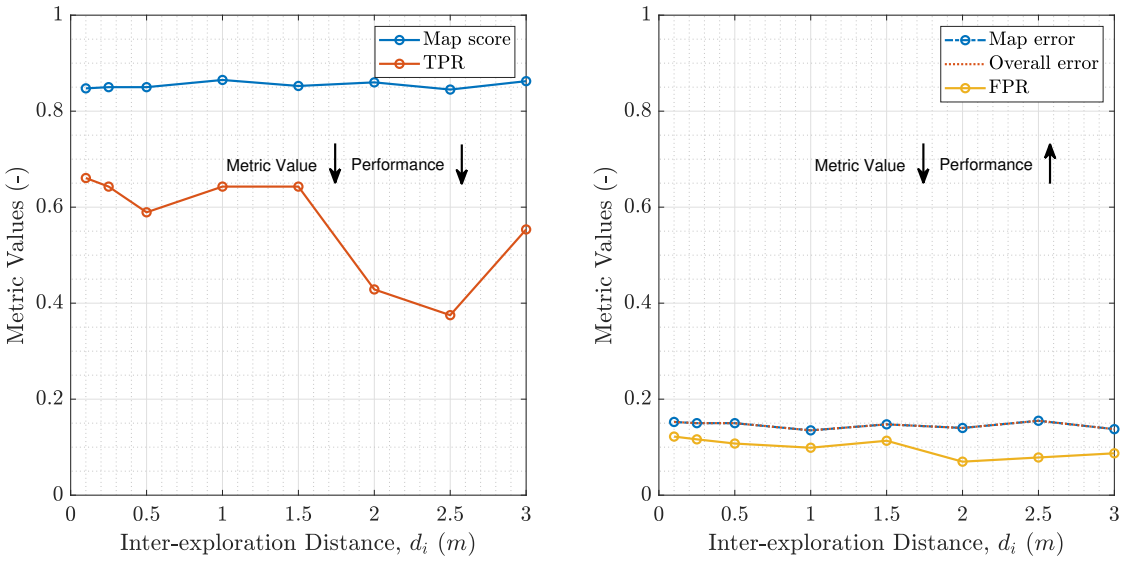

Figure 6.9: Metric values for the set of inter-exploration distances: (a) Normalized MS and TPR values, (b) ME, OE and FPR values for various occupancy maps generated for corresponding inter-exploration distance.

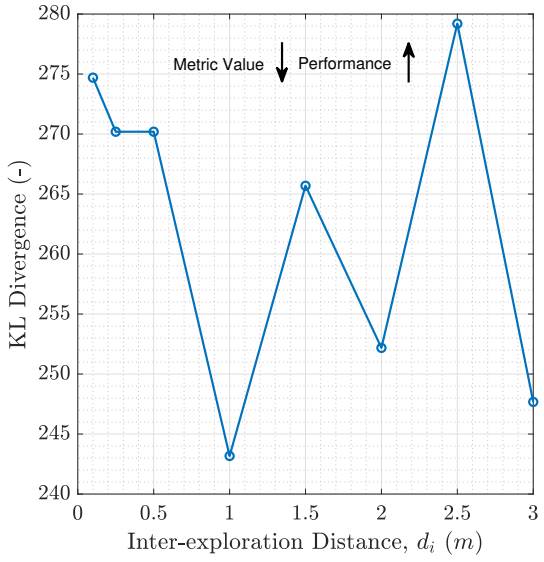

Figure 6.10: KL divergence values for various occupancy maps generated for corresponding inter-exploration distance.

Therefore, in addition to the indication of good performance by TPR for inter-exploration distances less than $1.5m$, the least FPR and KL divergence metric values for the map with the distance of $1m$

shows that the performance is good compared to the other chosen values.

6.5 Comparison of Maps Generated using ISM and FSM

This section compares the occupancy maps generated from the ISM and the FSM based methods by analyzing the metric values corresponding to the maps. Based on the analysis performed in the previous sections, the cell size of both the generated maps are set to $0.5m$. In addition to the cell size, the inter-exploration distance for both the methods are also set to $1m$ based on the analysis. The common simulation parameters mentioned in Tables 6.2 and 6.3 for the respective methods are maintained for this comparison as well. The generated occupancy maps are compared with their respective observable GT maps for the test scenario discussed in Section 6.2. The ISM generated map is binarized for evaluating the metrics based on the confusion matrix. For this binarization, a threshold of 0.5 is chosen. By choosing this threshold, if the probability of cells is greater than 0.5, then it is termed as occupied, or otherwise it is termed as empty.

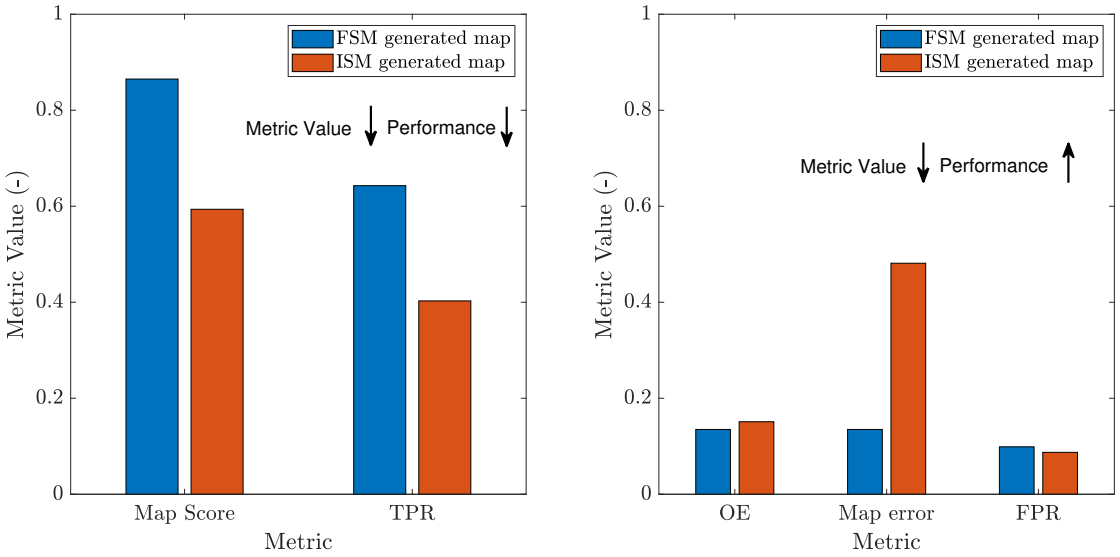

Figure 6.11: Evaluation of generated occupancy maps: (a) Normalized MS and TPR comparison, (b) OE, Normalized ME and FPR comparison for the generated occupancy maps.

Figure 6.11 shows the results of the metrics determined for the generated occupancy maps. Figure 6.11a shows the normalized MS compared for the two generated occupancy maps. Since the MS is directly dependent on the performance, clearly the figure shows that the FSM based method performs better than the ISM based method. This is also supported by normalized ME shown in Figure 6.11b. The high normalized ME metric for the map generated by the ISM based methods indicates that this method performs poorly compared to the FSM based method. However, the high ME for the map generated by the ISM based method is attributed to the initial probability value of 0.5 for all the map cells.

Figure 6.11a shows the TPR obtained for the generated maps. Here, the FSM based method has a slightly high TPR compared to the ISM based method. This suggests that the FSM based method judges the real occupied cells better than the ISM. Nevertheless, the FSM based method also has a high FPR compared to the ISM based method. This implies that the FSM based method has a high tendency to judge the occupied space correctly and wrongly compared to the ISM based method. Due to this tendency, the OE is high for the FSM based method compared to the ISM based method. To have a better visualization of the TP and FP classified cells compared to the GT map, more plots are reported in Appendix D.

Although MS and ME show that FSM based method performs exceptionally well compared to the ISM based method, the initial conditions for the ISM based method also play an important role in the setback. After binarizing the ISM generated map, the confusion matrix based metrics show that this method has less tendency to judge occupied cells incorrectly. This characteristic of the ISM based method along with its simplicity in implementation proves to be as effective as the FSM based method.

6.6 Conclusion

The performance of the mapping algorithms are analyzed for varying values of the chosen parameters. Grid resolution of the generated occupancy map is solely dependent on the cell size of the occupancy grid maps. The ISM based method does not show drastic influence of cell size on the overall performance. However, the TPR, FPR and the UR explained the influence of the cell size on the performance. On the other hand, the FSM based method shows deteriorating performance with increase in cell size. Nevertheless, for fine resolution maps, the computation time increases as the number of cells increases for a fixed map size in this method.

In addition to the grid resolution, the variation of inter-exploration distance is also considered in the performance analysis of the occupancy map algorithms. It is observed that for very low inter-exploration distances, the KL divergence values are high for the ISM based method. This high divergence value indicate that the generated map does not have good match with the GT map. For large inter-exploration distances, both the mapping methods show less ability to detect the occupied spaces correctly. This characteristic is due to increase in unexplored area that are actually occupied. For the FSM based method, the TPR indicated good performance for low inter-exploration distances. However, analysis of FPR and KL divergence values show good performance for the map with $1m$ inter-exploration distance.

The values chosen for the cell size and the inter-exploration distance are deployed in the respective mapping methods. Finally, the generated occupancy maps from both the mapping methods are compared using the metric values. The MS, ME and TPR metrics show that the FSM based method performs exceptionally better than the ISM based method. However, considering the ease of implementation of the ISM based method and its low tendency to judge occupied cells incorrectly, this method is as effective as the FSM based method.

Chapter 7

Conclusion and Recommendations

The main focus of this project was on mapping for an autonomous vehicle in a parking environment using the ultrasonic sensors. This chapter provides the final remarks in Section 7.1 and the recommendation for further research in Section 7.2.

7.1 Conclusion

The main research question that was defined earlier is: "Which mapping algorithm provides an effective map representation of the static environment using multiple ultrasonic sensors?". The two predominantly used OG mapping methods identified to address the problem of environment perception are inverse sensor model (ISM) based mapping and forward sensor model (FSM) based mapping methods. To understand how the ultrasonic sensors perceive the environment, the sensor characteristics are studied. The measurements from an ultrasonic sensor can be caused due to random and non-random phenomenon. Furthermore, the measurement can be affected by sensor noise, which also leads to measurement aberrations.

The ISM based method assumes that the occupancy state of a cell is independent of its neighboring cells. An ideal ISM model is constructed, which does not consider measurement aberrations. The recursive update equation derived using the Bayesian method involves less computation to fuse multiple sensor information. This update method is useful to obtain one coherent map of the environment. This method generates a probabilistic map, where each map cell is represented by probability values ranging from 0 to 1.

In the FSM based method, all the causes of a sensor measurement are considered. This method considers that the obstacle can be anywhere on the range surface within the sensor field of view (FoV). To incorporate the angular uncertainty and provide equal priority to the occupied cells at the same radial distance from the sensor position, the conventional FSM based algorithm is modified. A binary map representation of the environment is obtained due to decision of the occupancy state of a cell based on the comparison of the likelihood values.

The comparison of the generated maps with the ground truth (GT) map is performed using the metrics defined in the bench marking suite. The map score (MS) and the map error (ME) values are used for comparison on an overall level. The Kullback-Leibler (KL) divergence is a useful metric to measure

how bad the generated map estimates the occupancy states of the cells with respect to the bench-mark map. The metrics derived from the confusion matrix quantifies the overall error, sensitivity of an algorithm to judge occupied cells and the rate at which an algorithm wrongly judges an empty space as occupied.

The analysis of the influence of the grid resolution on the performance of the ISM based method shows that there is no drastic influence of the cell size on the overall performance. On the other hand, the FSM based method shows deteriorating performance with increase in cell size. Similarly, the analysis of the inter-exploration distance shows that both the mapping methods has less ability to detect the occupied spaces correctly for large distance values.

To finally answer the research question, the comparison of the mapping algorithms show that FSM based method has better overall performance and higher sensitivity of detecting the occupied cells. Considering the ease of implementation of the ISM based method and its low tendency to judge occupied cells incorrectly, this method is as effective as the FSM based method for ideal sensor measurements.

7.2 Recommendations

The mapping algorithms implemented in this project generates fairly accurate maps representing the environment. However, for practical use of the algorithms the following recommendations should be considered. In the ISM based method, the sensor model considered is for the ideal case of obtaining measurements without aberrations. This model can be improvised using machine learning algorithms with the knowledge of training sets. Using these algorithms a function can be developed, which accepts pose and sensor measurements as inputs and provides the occupancy probability as outputs [28].

The second recommendation is to obtain the values of the probability parameters used in the FSM using empirical methods. Another recommendation with respect to the FSM is to incorporate residual uncertainty in the resultant map representation in terms of probability values. The uncertainty map representation as opposed to binary map representation is useful for path planning and navigation [14, 27].

Although the metrics are useful for comparison of a generated map with the GT map at simulation level, the exact knowledge of the GT may not be available during practical implementation. Therefore, a benchmark map is necessary to compare the mapping algorithms. Furthermore, more test scenarios should be carried out for practical implementation.

Based on the implementation and evaluation of the occupancy mapping algorithms, each individual algorithm has its own strengths and weaknesses. Furthermore, both the algorithms complement each other with respect to computation and accuracy. Therefore, both the algorithms can be used to obtain one accurate map representation of the environment.

The last recommendation is to extend the mapping algorithm for dynamic obstacles and include the pose uncertainties. This inclusion can be essential for practical implementation. One of the methods to have knowledge of the dynamic obstacles is to incorporate a decay rate to the generated occupancy maps at a given instance. The decay rate can increase uncertainty in the map representation as time increases [41].

Bibliography

[1] "Automation and the nature of effort," Aug 2019. [Online]. Available: https://www.thinkautomation.com/automation-advice/automation-and-the-nature-of-effort/

[2] J. F. S. Cárdenas, J. G. Shin, and S. H. Kim, "A few critical human factors for developing sustainable autonomous driving technology," *Sustainability*, vol. 12, no. 7, 2020. [Online]. Available: https://www.mdpi.com/2071-1050/12/7/3030

[3] T. Litman, "Autonomous vehicle implementation predictions," *Victoria Transport Policy Institute*, vol. 28, no. 2014, 2014.

[4] M. Elbanhawi, M. Simic, and R. Jazar, "In the passenger seat: Investigating ride comfort measures in autonomous cars," *IEEE Intelligent Transportation Systems Magazine*, vol. 7, p. 4, 07 2015.

[5] T. van der Sande, J. Ploeg, and H. Nijmeijer, "Why is autonomous localisation required in lateral cooperative control?" *ERCIM News*, no. 109, pp. 34–35, 4 2017.

[6] "I-Cave – Integrated cooperative automated vehicles," library Catalog: i-cave.nl. [Online]. Available: https://i-cave.nl/

[7] R. Beekvelt, "I-CAVE project: Integration of a wheel speed measuring system and object detecting system. Internship Report." p. 69, Jan. 2020.

[8] "Understanding how ultrasonic sensors work," 2019, library Catalog: www.maxbotix.com. [Online]. Available: https://www.maxbotix.com/articles/how-ultrasonic-sensors-work.htm

[9] M. M. Kloompmakers, "Object tracking for autonomous and cooperative driving," *TU Eindhoven*, 2020.

[10] C. Fernández, "Grid-based multi-sensor fusion for on-road obstacle detection: Application to autonomous driving," 2015.

[11] L. Matthies and A. Elfes, "Integration of sonar and stereo range data using a grid-based representation," in *1988 IEEE International Conference on Robotics and Automation Proceedings*, Apr. 1988, pp. 727–733 vol.2.

[12] D. Joubert, "Adaptive occupancy grid mapping with measurement and pose uncertainty," *Department of Mathematical Sciences, Stellenbosch University*, p. 83, 2012.

[13] E. Szádeczky-Kardoss, B. Kiss, and I. Wahl, "Design of a semi-autonomous parking assist system," in *2009 European Control Conference (ECC)*, Aug. 2009, pp. 4949–4954, iSSN: null.

[14] D. Joubert, "Adaptive occupancy grid mapping with measurement and pose uncertainty," Ph.D. dissertation, Stellenbosch: Stellenbosch University, Dec 2012, accepted: 2012-11-27T07:39:08Z. [Online]. Available: https://scholar.sun.ac.za:443/handle/10019.1/71911

[15] S. Thrun, *Robotic mapping: a survey*. Morgan Kaufmann Publishers Inc., Jan 2003, p. 1–35.

[16] R. HoseinNezhad, B. Moshiri, and M. Asharif, "Sensor fusion for ultrasonic and laser arrays in mobile robotics: a comparative study of fuzzy, Dempster and Bayesian approaches," in *2002 IEEE SENSORS*, vol. 2, Jun. 2002, pp. 1682–1689 vol.2.

[17] A. Elfes, "Sonar-based real-world mapping and navigation," *IEEE Journal on Robotics and Automation*, vol. 3, no. 3, pp. 249–265, Jun. 1987, conference Name: IEEE Journal on Robotics and Automation.

[18] A. Elfes, "Occupancy Grids: A Stochastic Spatial Representation for Active Robot Perception," *ArXiv*, 2013.

[19] S. Thrun, "Learning occupancy grid maps with forward sensor models," *Auton. Robots*, vol. 15, no. 2, p. 111–127, Sep. 2003. [Online]. Available: https://doi.org/10.1023/A:1025584807625

[20] J. Carvalho, "Comparative Study of Inverse and Forward Sensor Models in Occupancy Grid Mapping Using Sonars," *Institute for Systems and Robotics*, p. 2, 2012.

[21] M. Salem, "Building an efficient occupancy grid map based on lidar data fusion for autonomous driving applications," 2019.

[22] T. Colleens, J. Colleens, and D. Ryan, "Occupancy grid mapping: An empirical evaluation," in *2007 Mediterranean Conference on Control Automation*, Jun. 2007, pp. 1–6.

[23] H. Moravec and A. Elfes, "High resolution maps from wide angle sonar," in *1985 IEEE International Conference on Robotics and Automation Proceedings*, vol. 2, Mar. 1985, pp. 116–121.

[24] S. Thrun, "Exploration and model building in mobile robot domains," in *IEEE International Conference on Neural Networks*, Mar. 1993, pp. 175–180 vol.1.

[25] K. Konolige, "Improved Occupancy Grids for Map Building," *Autonomous Robots*, p. 17, 1997.

[26] R. Grewe, M. Komar, A. Hohm, S. Lueke, and H. Winner, "Evaluation method and results for the accuracy of an automotive occupancy grid," in *2012 IEEE International Conference on Vehicular Electronics and Safety (ICVES 2012)*, 2012, pp. 19–24.

[27] R. S. Merali and T. D. Barfoot, "Patch map: A benchmark for occupancy grid algorithm evaluation," in *2012 IEEE/RSJ International Conference on Intelligent Robots and Systems*, 2012, pp. 3481–3488.

[28] S. Thrun, W. Burgard, and D. Fox, "Probabilistic robotics, 2005," *Massachusetts Institute of Technology, USA*, 2005.

[29] H. Tijms, *Understanding Probability: Chance Rules in Everyday Life*, 2nd ed. Cambridge University Press, 2007.

[30] S. Ross, *A first course in probability*. Pearson, 2014.

[31] D. Jurafsky and J. H. Martin, *Speech and Language Processing: An Introduction to Natural Language Processing, Computational Linguistics, and Speech Recognition, Appendix A*, 1st ed. USA: Prentice Hall PTR, 2000.

[32] H. M. et al, "Markov chains — brilliant math & science wiki." [Online]. Available: https://brilliant.org/wiki/markov-chains/

[33] S. Kim, "Lecture slides of Machine Learning, Hidden Markov Models II. Carnegie Mellon University." [Online]. Available: /http://www.cs.cmu.edu/~10601b/slides/HMM2.pdf

[34] L. Chandrashekar, "Characteristics of sonar sensors for short range measurement," 11 2014.

[35] H. P. Moravec, "Sensor fusion in certainty grids for mobile robots," in *Sensor Devices and Systems for Robotics*, A. Casals, Ed. Springer Berlin Heidelberg, 1989, p. 253–276.

[36] D. P. Massa, "Choosing an ultrasonic sensor for proximity or distance measurement part 2." [Online]. Available: https://www.fierceelectronics.com/components/choosing-ultrasonic-sensor-for-proximity-or-distance-measurement-part-2-optimizing

[37] A. Howard and L. Kitchen, "Generating sonar maps in highly specular environments," in *In Proceedings of the Fourth International Conference on Control Automation Robotics and Vision*. Citeseer, 1996.

[38] R. Singh and K. S. Nagla, "Sonar sensor model for the precision measurement to generate robust occupancy grid map," *MAPAN*, vol. 34, no. 2, pp. 239–257, 2019.

[39] J. Carvalho and R. Ventura, "Comparative evaluation of occupancy grid mapping methods using sonar sensors," in *Pattern Recognition and Image Analysis*, J. M. Sanches, L. Micó, and J. S. Cardoso, Eds. Springer Berlin Heidelberg, 2013, p. 889–896.

[40] "Simple guide to confusion matrix terminology," March 2014, (accessed on 09/11/2020). [Online]. Available: https://www.dataschool.io/simple-guide-to-confusion-matrix-terminology/

[41] S. A. M. Coenen, J. J. M. Lunenburg, M. J. G. van de Molengraft, and M. Steinbuch, "A representation method based on the probability of collision for safe robot navigation in domestic environments," in *2014 IEEE/RSJ International Conference on Intelligent Robots and Systems*, 2014, pp. 4177–4183.

Appendix A

Modeling Angular Probability Distribution

A probability distribution for various angles varying from $-90\,\mathrm{deg}$ to $90\,\mathrm{deg}$ is modeled as a trapezoid to closely represent the observed characteristic of the ultrasonic sensor. Figure A.1 shows an example of trapezoidal probability distribution. An important rule to be considered while constructing a trapezoidal probability distribution is that the area under the probability distribution should be equal to 1. Therefore, the sides of the trapezoid are selected in a such a way that this rule is followed. Accordingly, the dimensions of the trapezoid are chosen as 1.5 and 0.86. Here, the dimensions correspond to larger base and the height of the trapezoid, respectively. Therefore, the angles are normalized as

$$\theta = \frac{90+\theta}{180}1.5. \tag{A.1}$$

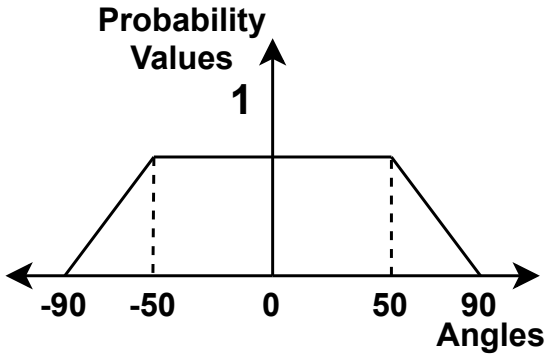

Figure A.1: Trapezoidal probability distribution.

The complete probability distribution for normalized angles is given as

$$p_{ang} = \begin{cases} \frac{\theta}{0.387209}, \text{if } 0 \leq \theta \leq 0.33, \\ 0.86, \text{if } 0.33 < \theta < 1.1667, \\ \frac{\theta - 1.5}{-0.3876}, \text{if } 1.667 \leq \theta \leq 1.5. \end{cases} \tag{A.2}$$

Appendix B

Results for Analysis of ISM for Various Cell Sizes

This appendix presents the results of the metrics determined at each update of the ISM generated map. The update of the generated map takes place for each new sensor measurement obtained. Figures B.1a and B.1b show the obtained normalized map score (MS) and normalized map error (ME) metric values at each update of the occupancy map for the various cell sizes. While the MS is directly dependent on the performance of the mapping algorithm, the ME is inversely dependent on the performance. It can be seen from the figures that the lines corresponding $0.1m$ and $0.2m$ cell sizes almost overlap initially and as the map updates, they do not deviate much from each other. This small deviation implies that very high map resolutions do not influence the overall performance significantly.

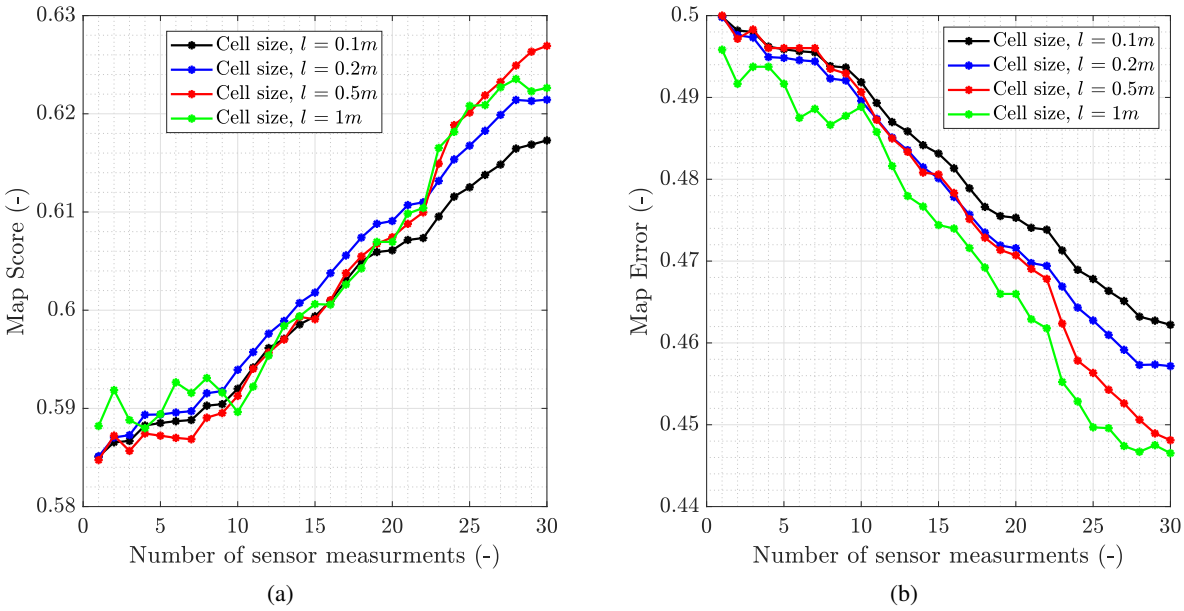

(a) (b)

Figure B.1: Metric values for the occupancy maps with different cell sizes: (a) normalized MS and (b) normalized ME values for various occupancy maps generated for corresponding cell sizes.

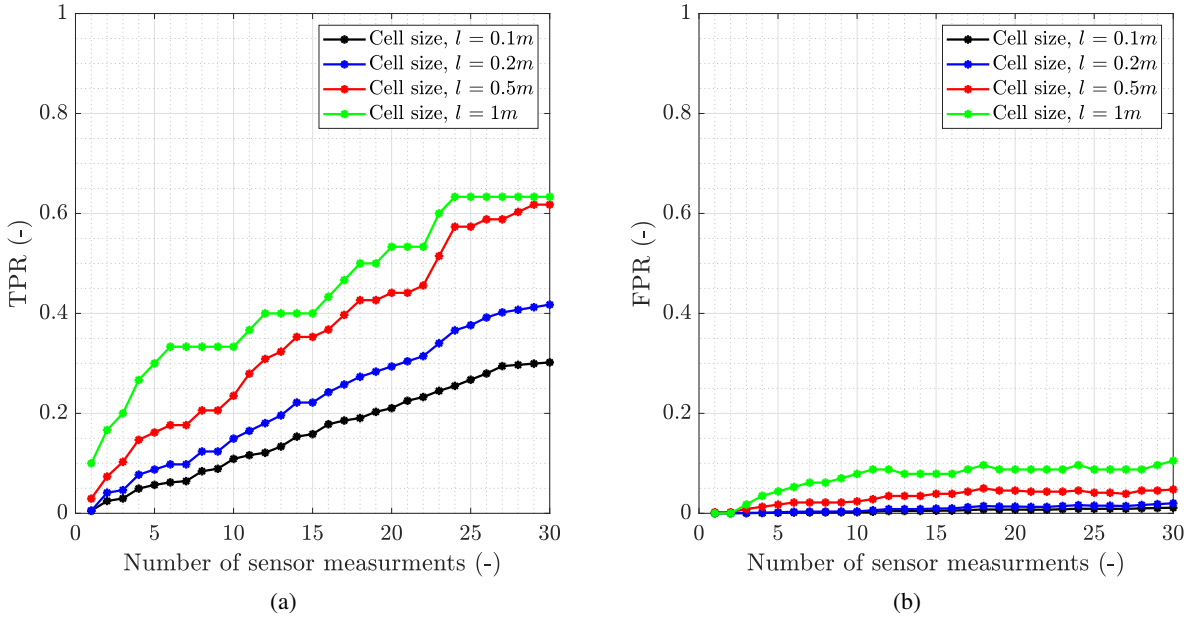

Figure B.2: Metric values for the occupancy maps with different cell sizes: (a) TPR and (b) FPR values for various occupancy maps generated for corresponding cell sizes.

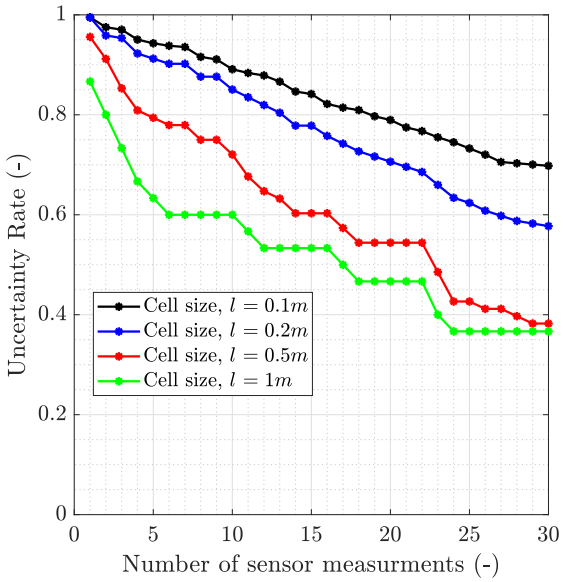

Figure B.3: Uncertainty rate for maps corresponding to the various grid resolutions.

In order to understand the nature of the overall performance lines corresponding to $0.5m$ and $1m$ cell sizes, the false positive rate (FPR) and the true positive rate (TPR) are investigated and shown in Figures B.2a and B.2b. FPR and TPR quantify the occupied cells that are wrongly and correctly judged, respectively. Clearly, the higher the FPR, the lower the performance of the occupancy grid map. In addition, Figure B.1a, shows improved performance for higher MS. Therefore, the drop in the

MSs are related to the increase in FPR at the same instance. On the other hand, the peaks in the MS are related to the surge in TPR. Similar to the MS, the behavior of the ME is explained with the help of the FPR and the TPR. The drop in the ME metric values are attributed to the rise in TPR whereas the peaks in the ME to the upward trend in the FPR.

Interestingly, Figures B.2a and B.2b show lower TPR and FPR values for small cell sizes. The lower range values of the metrics for small cell sizes attributes to the higher number of unexplored cells shown in Figure B.3. Clearly, the uncertainty rate lines corresponding to the low resolution maps fall below the lines corresponding to the high resolution maps. The higher uncertainty rates for the high resolution maps is due to fine discretization of the map. The effect of fine discretization is that even a very small unexplored region may result in occupancy of many cells uncertain.

Appendix C

Correlation between Grid Resolution and Inter-exploration Distance

This appendix provides the correlation between grid resolution and the inter-exploration distance while analyzing the influence of one of the parameters on the performance.

C.1 ISM Based Method

Figures C.1 and C.2 provides the results of the metrics for maps generated for various cell sizes with inter-exploration distance of $0.2m$ and $2m$, respectively. It can be seen that all the metric lines in Figure C.1 show similar trend to the corresponding metric lines in the Figure C.2.

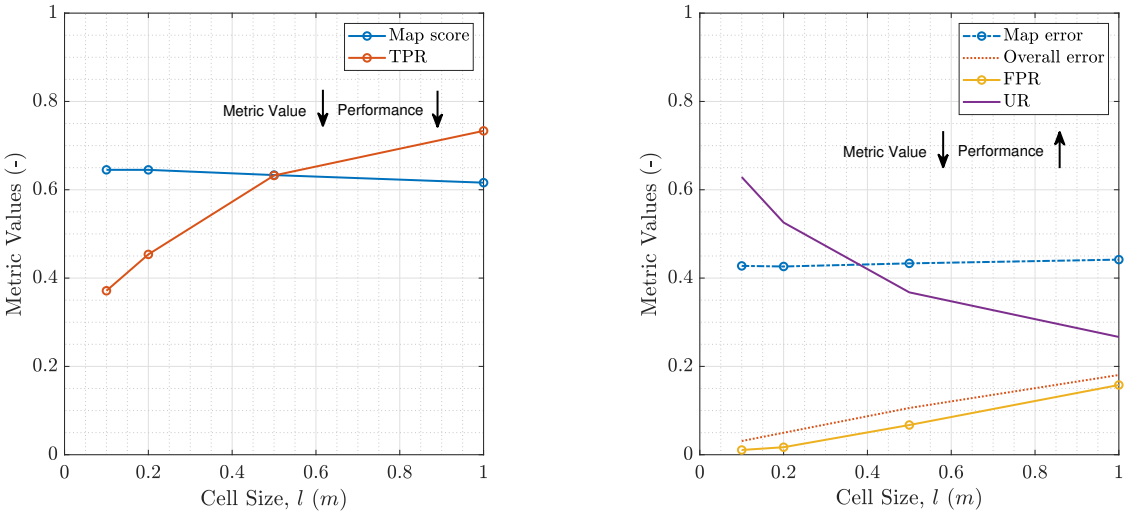

(a) (b)

Figure C.1: Metric values for the occupancy maps generated for various cell sizes with inter-exploration distance fixed as $0.2m$ (a) MS and TPR (b) ME, OE, FPR, UR.

Though there is not much change in trend in the metric lines, the metric values are not the same for the different inter-exploration distances. Therefore, inter-exploration distance also affects the performance but is not correlated to other parameter while analyzing performance.

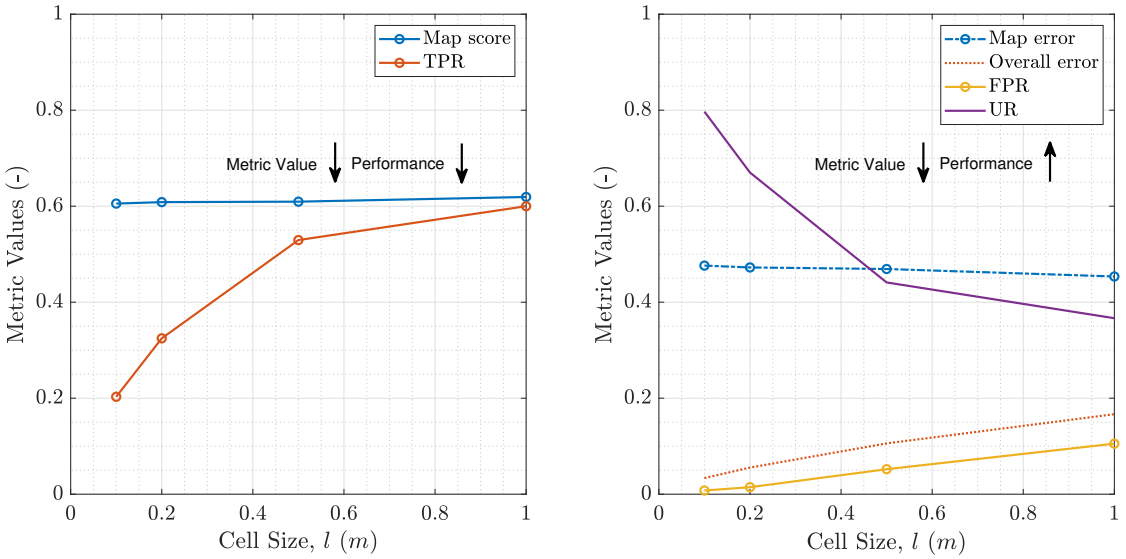

(a) (b)

Figure C.2: Metric values for the occupancy maps generated for various cell sizes with inter-exploration distance fixed as $2m$ (a) MS and TPR (b) ME, OE, FPR, UR.

C.2 FSM Based Method

Figures C.3a and C.4 provides the results of the metrics for maps generated for various cell sizes with inter-exploration distance of $1m$ and $2m$, respectively. The trend of metric values does not change with different inter-exploration distances. However, the performance deteriorates as the inter-exploration distance increases.

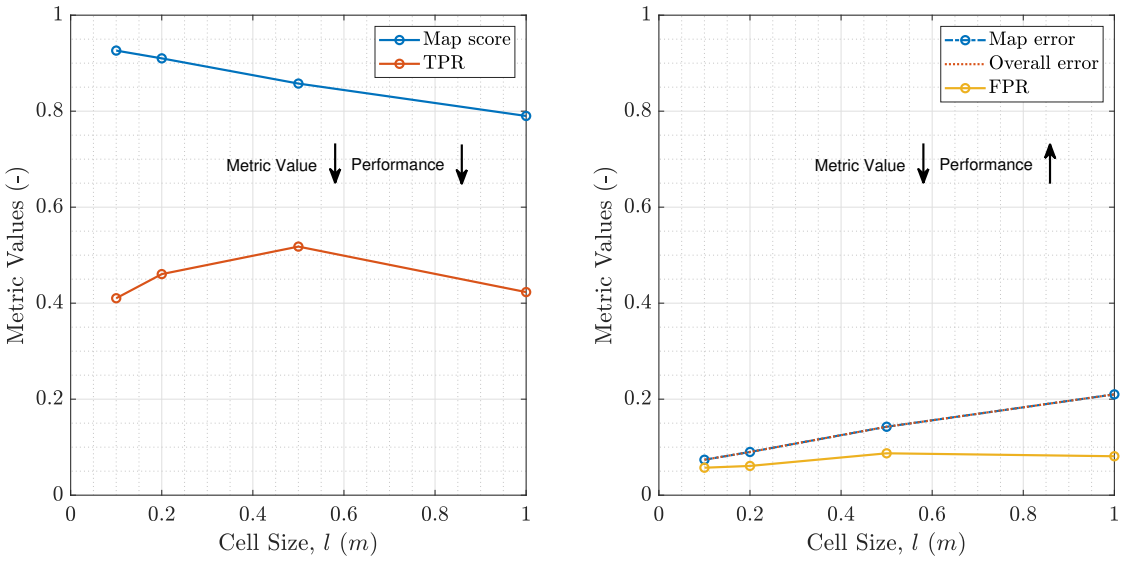

Figure C.3: Metric values for the set of cell sizes: (a) Normalized MS and TPR values, (b) Normalized ME, OE and FPR values for various occupancy maps generated for corresponding cell sizes.

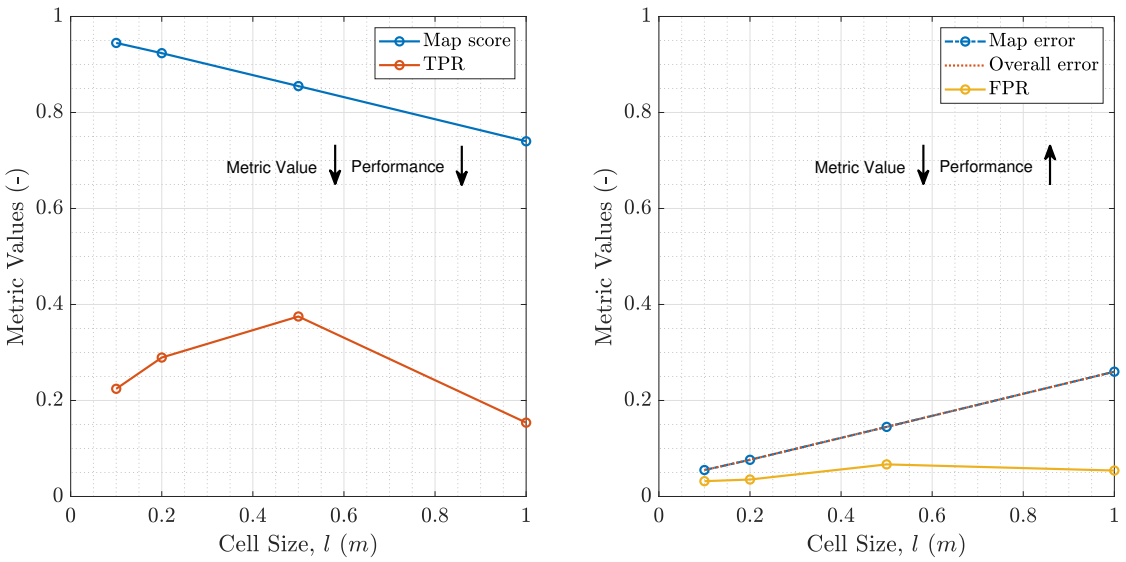

Figure C.4: Metric values for the occupancy maps generated for various cell sizes with inter-exploration distance fixed as $2m$ (a) MS and TPR (b) ME, OE, FPR, UR.

Appendix D

Generated Occupancy Maps

This appendix provides the results of occupancy maps generated from ISM and the FSM for a test scenario.

D.1 ISM Generated Map

In this section, the results of ISM generated map are presented for the test scenario as shown in figure D.1a. Figure D.1b shows the generated occupancy maps after exploration. The map generated from ISM is in the form of probability values corresponding to the occupancy of each cell in the map. This map is binarized based on a threshold value of 0.5 to check for its accuracy. Therefore, all the cells having a probability value less than or equal to 0.5 are assigned empty and the cells having probability higher than 0.5 are assigned occupied. Using the binarized map, the occupied cells are overlapped with the observable GT map, as shown in Figure D.2. The cells correctly classified by the ISM are in green color, whereas the incorrectly classified cells are in red dots.

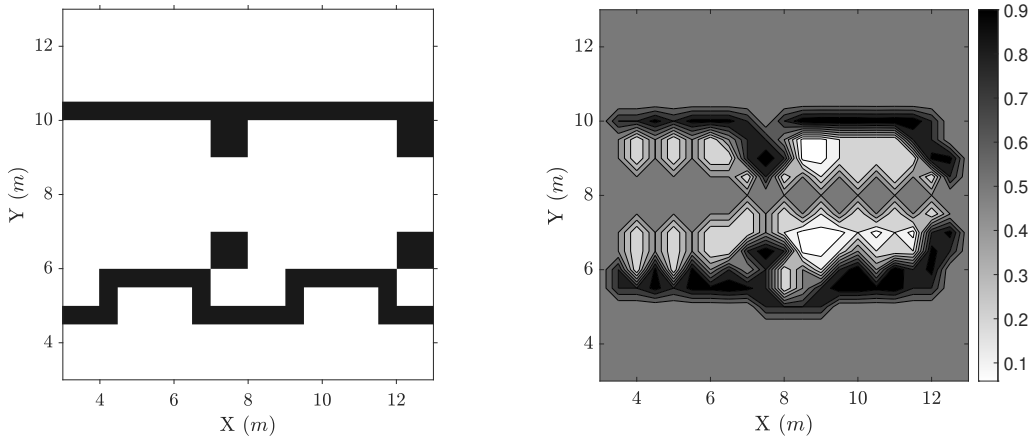

Figure D.1: Occupancy Maps: (a) observable GT map (b) ISM generated map.

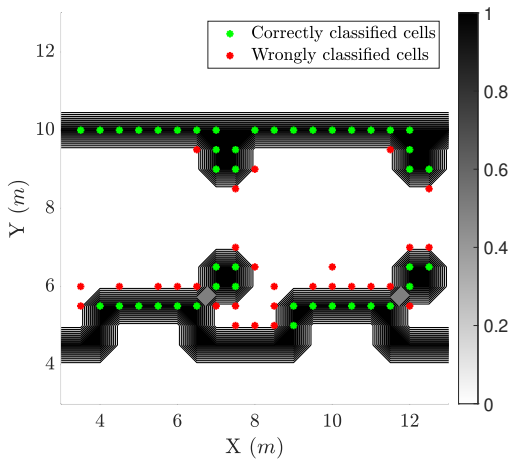

Figure D.2: True positive and false positive cells overlapped on the observable GT map.

D.2 FSM Generated map

In this section, the FSM generated map is presented for the chosen physical environment. The observable GT map representing the physical environment is shown in Figure D.3a. Figure D.3b shows the FSM generated map overlapped on the measurement cones obtained during the exploration. Since the generated map is already in binary form, the TP and FP classified cells are overlapped on the observable GT map, as shown in Figure D.4. Due to the consideration of noise variance, a lot of cells have been classified as occupied by the FSM. Hence the number of wrongly occupied classified cells are high in number for this method.

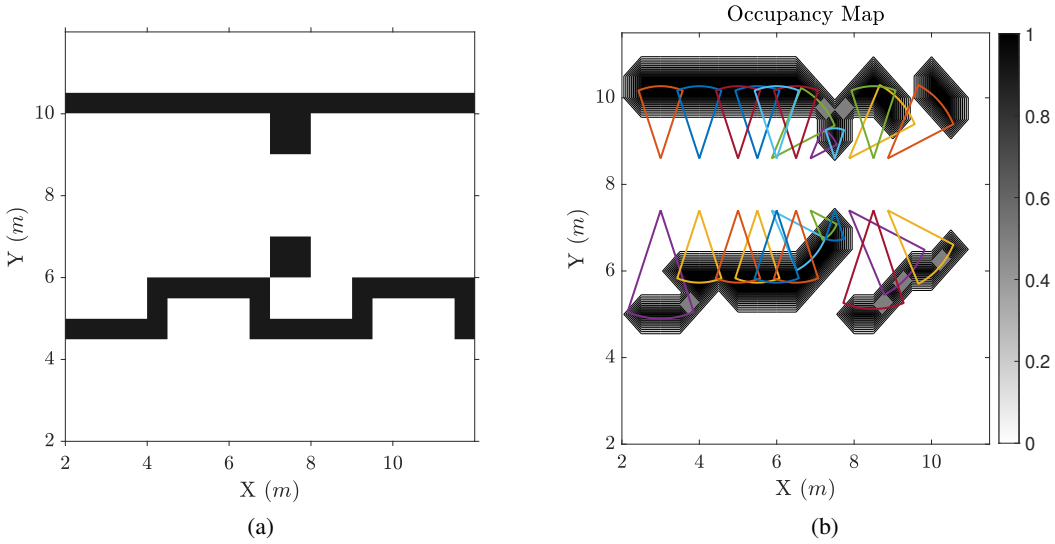

Figure D.3: Occupancy Maps: (a) observable GT map (b) FSM generated map overlapped on measurement cones of the sensor.

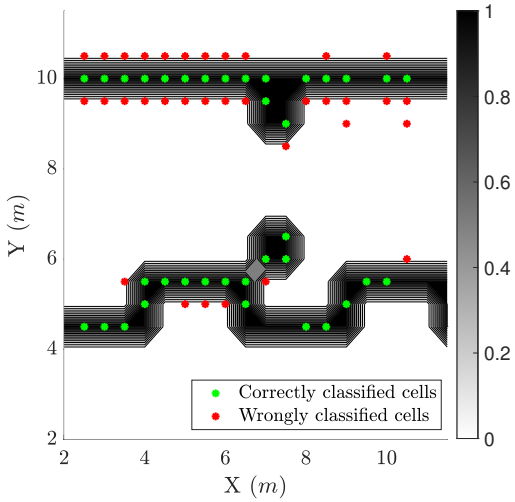

Figure D.4: True positive and false positive cells overlapped on the observable GT map.